NIRS

HIMAC

Dosimetry and Spectrometry of

Cosmic-ray Neutrons in Aircraft

(DOSCONA Experiment)

**Takashi Nakamura, Hiroshi Yasuda, Masashi Takada,
Kazuaki Yajima, Tatsuhiko Sato, Toru Fujishima**

2011 年 12 月
December 2011

(独) 放射線医学総合研究所
〒263-8555 千葉市稲毛区穴川 4-9-1

National Institute of Radiological Sciences
9-1 Anagawa 4-chome, Inage-ku, Chiba 263-8555, JAPAN

Dosimetry and Spectrometry of Cosmic-ray Neutrons in Aircraft
(DOSCONA Experiment)

Contents:

Preface

This report presents the results of in-flight measurements and related studies that were supported in part by the "Ground-based Research Program for Space Utilization" promoted by Japan Space Forum (JSF) and organized by the Japan Aerospace Exploration Agency (JAXA). The core members of this study, as listed below, are responsible for the contents of this report as authors.

Takashi Nakamura
Cyclotron and Radioisotope Center, Tohoku University, Sendai Japan

Masashi Takada*
National Institute of Radiological Sciences, Chiba, Japan

Tatsuhiko Sato
Japan Atomic Energy Agency, Ibaraki, Japan

Hiroshi Yasuda
National Institute of Radiological Sciences, Chiba, Japan

Kazuaki Yajima
National Institute of Radiological Sciences, Chiba, Japan

Toru Fujishima
Japan Space Forum, Otemachi, Japan

*For correspondence (m_takada@nirs.go.jp)

Abstract

Exact information on the cosmic-ray environment in spacecraft and aircraft are important for radiological protection of astronauts and aircraft crew. They are exposed to various types of primary and secondary cosmic-ray particles having the broad energy ranges. These particles could react in complicated manners inside a crew body and such reactions at deep organs would bring some critical adverse effects on the crew's health. To discuss this risk, it is necessary to know the accurate energy spectra and its spatial distribution of each species of cosmic-ray particles, particularly penetrating components such as high-energy neutrons which occupy a considerable fraction of total dose. It is very difficult, however, to precisely measure the neutrons with energies greater than 10-20 MeV because they are mixed with and hardly separated from co-existing particles such as protons and muons in the thin atmospheric environment.

Under these circumferences, we repeated in-flight measurements of cosmic-ray neutrons onboard a business jet aircraft near Japan from 2006 to 2008, during the solar minimum. The onboard experiments were supported as the 8th Ground-based Research Program for Space Utilization promoted by Japan Space Forum; this program was operated with a financial support of Japan Aerospace Exploration Agency (JAXA). The experimental flights were operated by Diamond Air Service Inc.

For cosmic-ray neutron measurements, we employed several neutron monitors including an original, newly developed neutron spectrometer. The spectrometer probe is a phoswich-type scintillation detector and can measure a high-energy neutron spectrum from 10 MeV to about 200 MeV, by separating well from cosmic-ray protons and others. It was an important object of this study to verify the effectiveness of this spectrometer at high altitude.

As results of the onboard measurements using selected rem counters, it was verified that cosmic-ray neutron doses can be successfully determined by numerical model simulations using the PHITS-based analytical model (PARMA). Also, it was confirmed that the new spectrometer works well for the determination of cosmic-ray neutron spectrum in the energy range from 10 to 200 MeV. The obtained spectrum of the high-energy neutrons was well connected with that of the low-to-middle energy neutrons (<15 MeV) evaluated with the Bonner ball neutron spectrometer. This is the first successful onboard experiment in which energy spectrum of neutrons with a wide energy range from thermal to about 200 MeV was presented with high energy resolution.

The obtained peak of the high-energy neutrons, however, appeared around 70 MeV which is considerably lower than those (about 100 MeV) reported in previous Bonner ball measurements, though this result agrees well with the neutron spectra measured with organic liquid scintillator on the ground and with double-scatter neutron telescope at the top of atmosphere. Though this discrepancy was discussed in comparison with model simulations in the present study, further discussion is strongly required by performing onboard long-haul flight measurements at high geomagnetic latitude. After such sufficient verification, tests on the International Space Station are desirable with developing a more sophisticated instruments regarding safety, energy efficiency and transportability.

Contents

1. Introduction

When primary cosmic rays consisting of galactic cosmic rays and solar particles come into the earth's atmosphere, secondary neutrons generated through nuclear cascade reactions with atmospheric atoms reach the ground. Over the past 10 years, there has been increasing concern about the exposure of aircraft crew to atmospheric cosmic radiation. At aviation altitudes of commercial jet aircrafts (around 11 km), cosmic-ray neutrons contribute about half of effective dose.

Whereas, dense accumulation of the semiconductor device greatly increases and the soft-errors of SRAM and DRAM on the ground level caused by high-energy cosmic-ray neutrons become a serious problem in the world (Nakamura et al. 2008). Under these circumstances, many neutron measurements onboard aircrafts and on the ground at different elevations have been carried out in Europe and North America (Schrewe 2000, Lewis et al. 2001, 2004; Goldhagen et al. 2002; EURADOS 2004), mainly at high geomagnetic latitudes. At low geomagnetic latitude, however, a few measurements have been successfully done onboard an aircraft over Japan (e.g. Nakamura et al. 1987). These measurements were all performed with a multi-moderator spectrometer, so-called 'Bonner ball detector', or a dose equivalent counter, so-called 'rem counter'. The Bonner ball detector has been widely used for neutron spectrometry due to its simple responses covering a certain energy range of neutrons from thermal to several MeV. Its energy resolution is not good, however, especially in the high energy region above 10 MeV; the energy spectrum in this region is strongly dependent on the initial guess spectrum. Regarding a rem counter, its simple handling feature and transportability are preferable for use in aircraft though it only gives a value of neutron ambient dose equivalent.

With expanding human space activities, precise neutron measurements are becoming important for radiological protection of astronauts. Most of the neutrons are produced from primary cosmic-ray charged particles passing through a space vehicle including wall, equipments, luggage, fuel, water and so on. But, it is very difficult to measure neutrons selectively in spacecraft where various radiation particles such as neutrons, protons, muons, pions, electrons and photons having wide energy ranges are mixed. There have been only a few measurements of neutron spectra below about 10 MeV with the Bonner ball neutron detectors (BBND) which was fabricated by the National Space Development Agency (NASDA, now JAXA: Japan Aerospace Exploration Agency). Using this system, Matsumoto et al. (2001) measured the neutron energy spectrum in the Space Shuttle in the 8th Shuttle-Mir mission (S/MM-08/STS-89) from January 24 to 28, 1998. A similar type of this Bonner ball detector was also used in the US module of ISS (International Space Station) flying at about 400 km in altitude to measure neutron dose from March 23 to July 6, 2001 (Koshiishi et al. 2007). Contribution of high-energy neutrons (> 10 MeV), however, is still uncertain and to be desirably

verified in future missions.

The energetic neutrons can penetrate deep into a crew body and could react in complicated ways at deep organs, which would bring some critical effects on the crew's health. To discuss this effect, it is necessary to know the accurate energy spectra and its spatial distribution of high-energy neutrons. It is very difficult, however, to precisely measure energetic neutrons in spacecraft or aircraft because they are mixed with and hardly separated from co-existing protons at high altitude. It is now desirable to verify the energy spectrum of neutrons with energies greater than 10 MeV by measurements with an advanced neutron spectrometer which can detect high-energy neutrons selectively and precisely.

2. Aim of this study

Under this circumference, we employed several neutron detectors including a newly developed original spectrometer to know the contribution of high-energy neutrons to cosmic radiation doses in spacecraft and aircraft. The detectors include neutron rem counters, liquid scintillation detector, Bonner-ball neutron detector and an original phoswich-type neutron spectrometer which is designed to measure high-energy neutron spectrum over 10 MeV up to a few 100 MeV selectively, separated from co-existing protons and other cosmic-ray particles. It is one of the important objects in this study to verify the effectiveness of this spectrometer at high altitude.

We had already made a phoswich-type scintillation detector composed of slow-decay plastic scintillator (NE115) and fast-decay liquid scintillator (NE213) (Takada et al, 1998, 2001, 2002, 2004, Takada and Nakamura 2007). Thick xylene-based liquid scintillator, NE213, having high sensitivity to neutral particles was surrounded by a thin plastic scintillator which should have a low sensitivity to neutrons. Charged particles are detected well by both scintillators.

For loading on a flying vehicle, however, the xylene solvent of the liquid scintillator was not preferable because of its toxicity and flammability. We thus tried to change the inner scintillator to lower toxic one. To obtain neutron energy spectrum on site, we developed an original data acquisition unit converting analog data of scintillation signals to digital data with 2ns intervals. Also, we developed a software program to display the optional signal integrals as two-dimensional plots on PC for particle discrimination and to analyze the energy spectrum from the selected data. This analyzing system designed exclusively for a scintillation detector is named by the authors as CREPAS (Cosmic Radiation and Energetic Particle Analyzing System). Furthermore, by combination of CREPAS and Bonner ball detector, we expect to obtain a whole energy spectrum of cosmic-ray neutrons in space and aviation.

3. Materials and Methods

In this section, detector specifications, flight experiment conditions and the features of atmospheric radiation models are described. We employed several radiation instruments for cosmic-ray neutron measurements at high altitude. They were installed in a business jet aircraft and flown around the middle part of Japan. The results obtained were compared to numerical simulations using a newly developed analytical model based on the Monte Carlo simulations.

3-1. Detectors

3-1-1. Neutron Rem Counters

Three commercial products of neutron rem counter were chosen for in-flight measurements of 1 cm ambient dose equivalent, H*(10): (1) a conventional moderating rem meter composed of a 5.1 cm-diam ^{3}He proportional counter and a 25 cm-diam polyethylene sphere (NCN1, Fuji Electronics Systems), (2) an extended energy-range rem meter of a ^{3}He counter with a tungsten powder shell (WENDI-II, Ludlum Measurements Inc.) and (3) a proton-recoil scintillation rem meter of ZnS phosphor with ^{6}Li (PRESCILA, Ludlum Measurements Inc.). All these monitors are commercially available and transportable. The major physical properties of these monitors are summarized in **Table 3.1.1.1**. As to the NCN1 and WENDI-II, the H*(10) value is determined by multiplying a constant conversion coefficient and pulse counts generated from the ^{3}He(n,α)Li reaction with thermalized neutrons. The dose value of the PRESCILA is determined from signal counts of recoil protons generated by incident energetic neutrons in the ZnS scintillator. Threshold setting for n/γ discrimination was given as a default, and low sensitivity to photons was confirmed using ^{60}Co and ^{137}Cs gamma-ray sources. Detailed dosimetric properties regarding the NCN1 have been introduced by Nakane et al. (2004) and those for the WENDI-II and PRESCILA have been reported by Olsher et al. (2000, 2004, 2008). The data of the NCN1 were recorded to an original data logger developed by the authors and those of the WENDI-II and PRESCILA were saved to a commercial data logger (Model 2350-1, Ludlum Measurements Inc.).

Pulse counts recorded in the data loggers were read out to a personal computer after landing and they were converted to H*(10) values using constant conversion coefficients that had already been given for each detector according to calibration results obtained by the authors using ^{241}Am-Be source neutrons and 65 MeV p-^{7}Li neutrons produced in the cyclotron of Tohoku University, Japan. The obtained H*(10) values were compared to predicted neutron doses obtained with a PHITS-based analytical model "PARMA" (Sato et al. 2008) which will be explained in the section 3-3.

Table 3.1.1.1   Major physical properties of the three neutron monitors used in the present study.

Product name	Manufacturer	Physical properties			
		Detector	Moderator/ Reactor	Size [cm]*	Weight [kg]
NCN1	Fuji Electric Systems, Inc. (Japan)	ϕ1.5 cm ^{3}He proportional counter	Polyethylene (boron doped)	W25×D30×H40	10
WENDI-II	Ludlum Measurements, Inc. (US)	ϕ2.5 cm ^{3}He proportional counter	Polyethylene +Tungsten power shell	ϕ23×H32	14
PRESCILA	Ludlum Measurements, Inc. (US)	ZnS scintillator and ^{6}LiF	Polyethylene (boron doped)	W11×D11×H26	2.0

*The NCN1 was connected to an original data logger with a size of W8.0×D2.5×H12 cm^3; the WENDI-II and the PRESCILA were connected to an exclusive data logger (Model 2350-1, Ludlum Measurements Inc.) with a size of W11×D22×H15 cm^3 and a weight of 2.3 kg including batteries.

3-1-2. DARWIN

DARWIN, Dose monitoring system Applicable to various Radiations with WIde energy raNges, is composed of a scintillation detector which consists of layered scintillators and a data acquisition system. The detail features of DARWIN have been described in previous reports (Sato et al. 2005; 2007). DARWIN is designed to be used in monitoring doses in workspaces of high-energy accelerator facilities, and it cannot distinguish scintillations from protons and those from neutrons. Thus, we need to correct neutron dose values measured with DARWIN at flight altitudes by excluding the contamination induced by protons.

System

The schematic view of DARWIN is illustrated in Fig. 3.1.2.1. DARWIN is composed of [1] a phoswitch-type scintillation detector, which consists of liquid organic scintillator BC501A coupled with ZnS(Ag) scintillation sheets doped with ^{6}Li, and [2] a data acquisition system based on a Digital-Storage-Oscilloscope (DSO). It is capable of measuring doses from neutrons, photons and muons with energy ranges from thermal energy to 1 GeV, 150 keV to 100 MeV, and

1 MeV to 100 GeV, respectively. Dose from neutrons below 1 keV is evaluated from the number of scintillations in the ZnS(Ag) sheets, while those from neutrons above 1 keV as well as photons and muons are estimated from the light outputs of scintillations from BC501A by applying the G-function method (Oyama et al. 1994) which directly relates the light output to the corresponding dose.

In this system, signals from the phoswitch detector were digitized by the analog-to-digital converters (ADCs) equipped in DSO, and stored in the memory allocated in ADC. The stored waveform data were transferred to the memory allocated in Windows^{TM} by every 1000 events, and analyzed by a Windows dynamic link library (DLL) driven by a LabVIEW^{TM} program for determining the trigger particle type and the light outputs of the scintillations. In the waveform analysis, each scintillation was identified as that triggered by the incidence of neutron, photon and muon (hereafter referred to neutron, photon and muon scintillation, respectively) by means of the pulse shape and height discrimination (PSHD) technique (T. Sato et al. 2005). The neutron scintillations were further distinguished between those from the ^{6}Li-doped ZnS(Ag) sheet stimulated by α particle produced by ^{6}Li(n, α) reactions, and from the BC501A stimulated by proton, deuteron or α particle stopped in the detector produced by neutron-induced nuclear reactions. Signals from photon and muon scintillations were discriminated by their pulse heights, since their pulse shapes were almost identical to each other. In the pulse height discrimination, we assumed that scintillations with light outputs below and above 8 MeVee were regarded as the photon and muon scintillations, respectively. The obtained light output of each scintillation was converted to the corresponding dose in real-time by the LabVIEW program, applying the G-function method (Oyama et al. 1994).
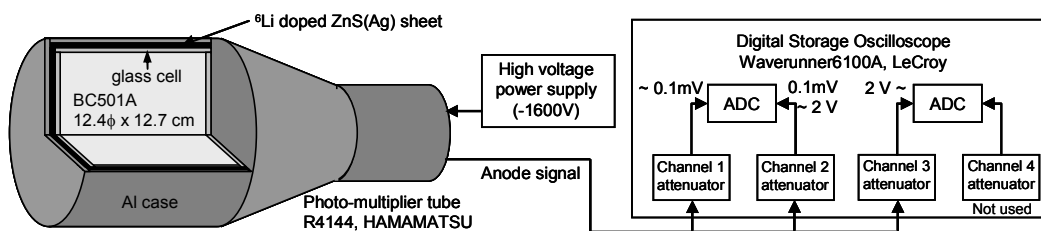

Fig.3.1.2.1. Schematic view of DARWIN.

Data Correction

The radiation fields at high altitudes, however, consist of not only neutron, photon and muon but also electron, positron and proton. When an electron or positron strikes into the detector, it creates a signal that is identified as photon or muon scintillation by PSHD. For scintillations

with the same light output, the corresponding doses estimated from the G-functions for the electron or positron are generally larger and smaller than those for the photon and muon, respectively, since the G-functions are significantly related to their fluence to dose conversion coefficients. Thus, electron or positron doses evaluated from the scintillations miss-identified as the photon and muon scintillations are underestimated and overestimated, respectively. In the total dose estimation, the error associated with this miss-identification is expected to be not so considerable – at most 15%, since the underestimation and overestimation cancel each other.

The scintillation triggered by the direct incidence of proton that stops in the detector is identified as the neutron scintillation by PSHD. This proton contamination should be excluded from the measured neutron dose rates. We therefore corrected the measured neutron dose rates by DARWIN, D_M, by introducing a correction factor C as written by:

$$D_C = D_M C = D_M \left(\frac{d_N}{d_N + d_P} \right),$$ (1)

where D_C denotes the corrected neutron dose rates, and d_N and d_P represent the neutron and stopped proton dose rates obtained from the G-function method, respectively. The numerical values of d_N and d_P can be estimated by

$$d_N = \iint R_N(E, L) \phi_N(E) G_N(E) \mathrm{d}E \mathrm{d}L$$

and

$$d_P = \iint R_P(E, L) \phi_P(E) G_N(E) \mathrm{d}E \mathrm{d}L,$$ (2)

where R_N and R_P are the response functions of BC501A for neutron and proton with energy E and light output L, ϕ and ϕ_P are the neutron and proton spectra, respectively, and G_N is the G-function for the neutron irradiation. Note that this correction is generally not necessary for dose monitoring in workspaces of high-energy accelerator facilities, since protons hardly exist in the radiation fields.

In the determination of the correction factor for the flight experiment, we adopted the response functions calculated by the SCINFUL-QMD code (D.Satoh et al. 2006) coupled with PHITS (Iwase et al. 2002), and the cosmic-ray spectra calculated by PARMA (T.Sato et al. 2008). It should be noted that the correction factor depends on the flight condition, and its maximum and minimum values are 0.94 and 0.91, respectively. The error associated with this correction is thus assumed to be at most several percents. In addition to this uncertainty, the experimental neutron dose rates also include the systematic error of approximately 10% due to the inadequate response of DARWIN to keV-order neutrons.

3-1-3. BBND

The Bonner Ball Neutron Detector (BBND) developed for use on board the International Space Station and the shuttle mission (Matsumoto et al. 2001; Koshiishi et al. 2007) was used for the cosmic-ray neutron energy spectrum measurement. It is a neutron spectrometer unit consisting of six Bonner-ball sensors, pre-amplifiers, analogue-to-digital converters, high-voltage power supplies, electrical circuits, an operation panel, data recording device and supporting equipment. We selected the BBND as a neutron spectrometer for this work because of its desirable features for our aircraft experiment, such as its simplicity of operation and solidity, coming from its original purpose of use in a space experiment.

Figure 3.1.3.1 shows a photograph of a BBND sensor, and Fig. 3.1.3.2 shows an internal view of the BBND unit. The neutron detector of the BBND is a proportional counter, 5.1 cm in diameter, filled with 6.1 atm Helium-3 gas (^{3}He counter). Sensor 1 is a bare ^{3}He counter. Sensor 2 is a ^{3}He counter covered with 1-mm-thick gadolinium. Sensor 3 is a ^{3}He counter covered with a 1.5-cm-thick polyethylene sphere and 1-mm-thick gadolinium. Sensors 4, 5 and 6 are ^{3}He counters covered with 3-, 5- and 9-cm-thick polyethylene spheres, respectively. The properties of Bonner ball sensors 1-6 installed in the BBND are listed in Table 3.1.3.1 and the energy response functions of each sensor are shown in Fig.3.1.3.3. More detailed information about the BBND is included in the paper of Matsumoto et al.(2001).

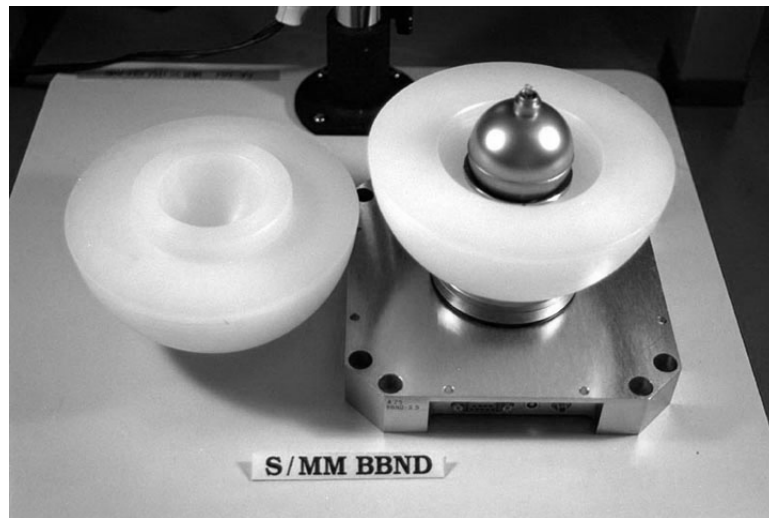Fig. 3.1.3.1   Photos of BBND. (C) NASA/JAXA

Fig. 3.1.3.2 Internal view of the BBND unit. (C) NASA/JAXA

The maximum entropy deconvolution code MAXED (Reginatto and Goldhagen 1998; 1999; Reginatto et al. 2002) was used for the unfolding code of this study (obtained as part of the UMG package). We input the response function of the BBND sensors (Bonner balls), the measured count rate of each sensor, the uncertainty of measured data and a default cosmic-ray neutron energy spectrum (default spectrum) calculated with PARMA into the MAXED program and obtained an unfolded neutron energy spectrum with the uncertainty of each energy bin.

Table 3.1.3.1   Major properties of BBND

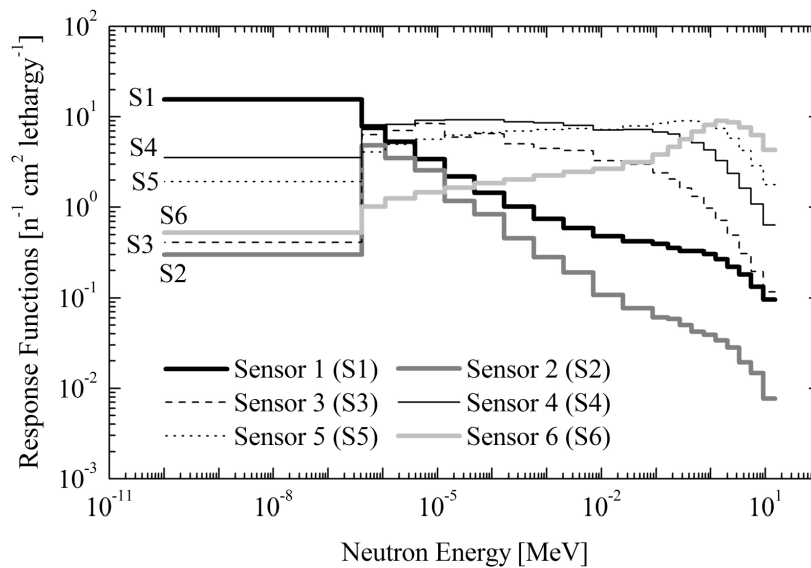| Bonner-ball detector ID	Diameter [cm]	Polyethylene-sphere thickness [cm]	Notes
Sensor 1	5.1		bare ^{3}He proportional counter
Sensor 2	5.1		covered with 1-mm-thick Gd
Sensor 3	8.1	1.5	covered with 1-mm-thick Gd
Sensor 4	11	3	
Sensor 5	15	5	
Sensor 6	23	9	

Fig. 3.1.3.3　Response functions of BBND sensors. The values are given by Matsumoto et al. (2001).

3-1-4. Phoswich Detector / CREPAS

Specification

To measure the energy spectrum of high-energy cosmic-ray neutrons in the atmosphere, we have newly developed an original neutron spectrometer with signal processing instruments (Takada et al 2010 former). The detector consists of an EJ309 organic liquid scintillator of 12.17 cm in diameter and 12.17 cm long covered with 15mm-thick EJ299-13 plastic scintillators as shown in Fig. 3.1.4.1. Both types of scintillators were fabricated by ELJEN Technology, TX, USA. The liquid scintillator can measure 1 to 180 MeV neutrons and 1 to 50 MeV photons. The outer plastic scintillator identifies incident charged particles. The properties of the EJ309 liquid scintillator are similar to those of the NE213 and BC501A scintillators. The densities and ratios of hydrogen and carbon atoms (H/C) of the EJ309 liquid and EJ299-13 plastic scintillators are 0.964 g/cm^3 and 1.25, and 1.035 g/cm^3 and 1.109, respectively. To allow long and safe onboard experiments, 2-mm-thick transparent acrylic liners are used between the inner and outer scintillators.
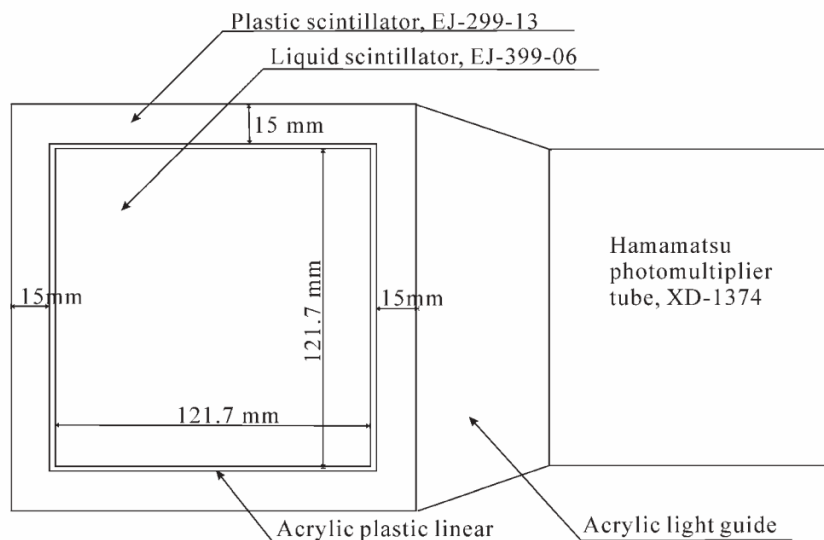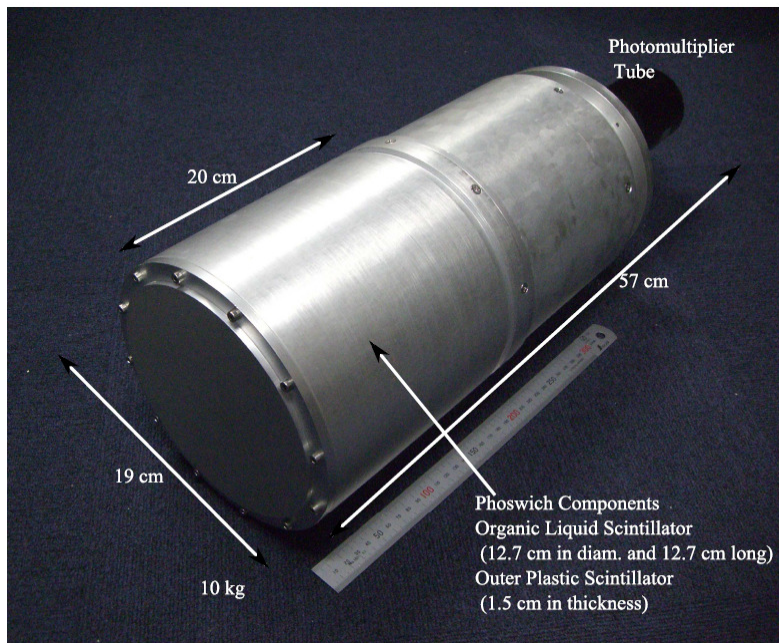
Fig. 3.1.4.1 A photo of the phoswich detector probe (above) and the schematic
structure of phoswich neutron detector composed of an inner EJ309 organic
liquid scintillator and an outer EJ299-13 plastic scintillator coupled to a
photomultiplier XD-1374 (below).

Similar to the NE213 scintillator, the EJ309 liquid scintillator can discriminate neutrons and
photons well. Both scintillators produce similar scintillations with decay times of 3.5 ns and 3.2
ns, respectively. In contrast, EJ299-13 produces scintillation with a longer decay time (285 ns)
than that of the widely used NE102A plastic scintillator (2.4 ns). The fabricated scintillator is

coupled with a photomultiplier 120 mm in diameter (R1250, Hamamatsu Photonics K.K., Japan) via an acrylic light guide ($C_8H_5O_2$: ρ=0.95 g/cm^3).　The signal rise time, gain, and pulse linearity are reported by the manufacturer to be 2.5 ns, 1.4 ×10^7, and 2% deviation up to 160 mA, respectively. The phoswich detector is operated at -1200 V to maintain light output linearity. The entire detector is 19 cm in diameter and 57 cm long and it weights 10 kg.

Particle discrimination procedure

The phoswich detector can measure neutron and photon events separately by discriminating charged-particle events in the mixed radiation field. Non-charged particles of neutrons and photons deposit their energies mainly in the inner liquid scintillator. On the other hand, charged particles deposit their energies in both the inner liquid and outer plastic scintillators. Both scintillators emit scintillations with much different decay times: 3.5 ns for liquid and 285 ns for plastic. Signals of neutron and photon events are derived from only the liquid scintillator, but those from charged particles are the sum of scintillations from both the liquid and plastic scintillators. Signals from non-charged and charged particles therefore have small and large tail components, respectively, which enable the identification of incident particles (Fig.3.1.4.2).
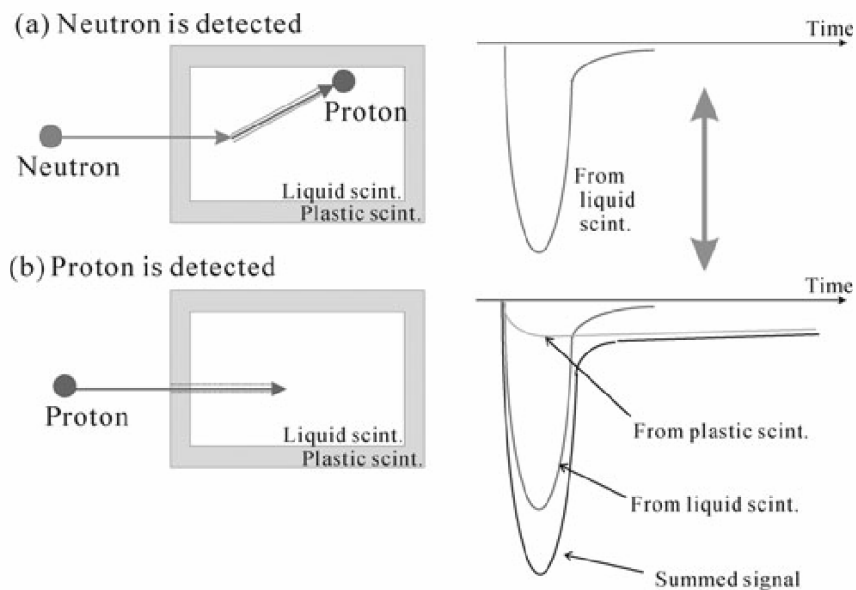

Fig.3.1.4.2 Particle discrimination method using a phoswich neutron detector; (a) and (b) show signals, when neutron and proton are detected. Neutron produces shorter signals; while, proton longer signals.

The charge of the signal was integrated over three gates. The integrated charges from 10 ns

advanced to 200 ns delayed from the rise of signal are called the total component charge. The integrated charges from 60 to 200 ns delayed and from 200 to 400 ns delayed from the rise of signal are called the slow and tail components, respectively. Two dimensional plots of the total and tail components, and the total and the ratio of slow to total components (slow/total component) observed using quasi-monoenergetic neutron beams produced from 70 MeV p-Li reactions at the Cyclotron and Radioisotope Center (CYRIC), Tohoku University, are shown in Figs. 3.1.4.3 (A) and (B), respectively. Non-charged particle events of neutrons and photons were discriminated from charged particle events using the boundary as shown in (A), and the neutron events were discriminated from photon events using the boundary shown in (B). The secondary particles of protons, alpha particles and electrons generated by incident particles (neutrons and photons) are shown in (B).
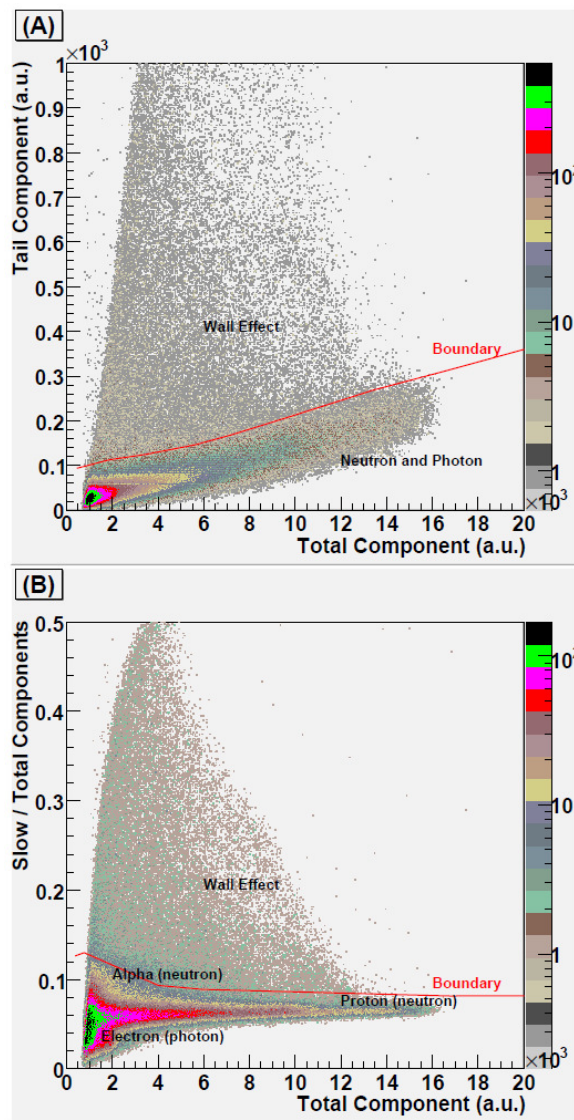

Fig. 3.1.4.3 Two-dimensional particle discrimination plots of total and tail components

(A) and the total and the ratio of slow to total components (B) measured with quasi-monoenergetic neutron beams produced from a 70 MeV p-Li reaction at CYRIC. Secondary particles produced by neutrons and photons, wall-effect events, and boundaries for particle discrimination are drawn.

High-energy protons recoiled by neutrons can escape out of the inner liquid scintillator and be detected in the outer plastic scintillator. The escaped protons are identified as incident charged particles even if the neutrons are incident to the detector. Neutrons and photons detected at the outer scintillator are identified as charged particles incident to the detector. Similarly, high-energy deuterons and helium-4 ions produced by neutrons, and photon-induced electrons that escape from the liquid scintillator are identified as charged particles. These events, shown in Fig. 3.1.4.3, are called wall effect events. The wall effect events were discriminated from neutron and photon events in the experiments. In the calculation, the wall effect is simulated by the coincidence of deposited energies in the inner liquid and outer plastic scintillators.

Neutron response functions

The neutron response functions of the phoswich detector were measured using a variety of quasi-monoenergetic neutron beams from 37 to 78 MeV at three cyclotron facilities, National Institute of Radiological Sciences (NIRS) (Honma 2007), CYRIC (Baba 2006) and the Takasaki Ion Accelerators for Advanced Radiation Application (TIARA) of the Japan Atomic Energy Agency (JAEA) (Baba et al. 1999). Quasi-monoenergetic neutron beams were produced by bombarding 40, 48, 70 and 80 MeV proton beams onto thin lithium targets with 2 MeV energy losses at NIRS and TIARA, and 5 MeV energy losses at CYRIC. Protons transmitted through the target without any reaction were diverted by a bending magnet into a beam dump. Neutrons in the 0 degree direction were guided to the experimental room through collimators at the CYRIC and TIARA neutron beam facilities. Scattered neutrons around the target chamber, and photons produced at the target and beam dump were measured and deemed to be negligible.

The quasi-monoenergetic neutron spectra were measured with the TOF method (Baba et al. 1999; 2006) as shown in Fig. 3.1.4.4. Neutron peak energies were measured to be 36.9, 46.0, 64.9 and 77.1 MeV for the 40, 48, 70 and 80 MeV p-Li reactions, respectively, with peak widths in FWHM from 2.4 to 6.1 MeV as shown in Table 3.1.4.1. The 64.9 MeV neutron peak at CYRIC was much larger and broader than the other peaks due to the usage of the thicker Li target. The spectra consist of a monoenergy peak due to the ^{7}Li(p, n$_{0,1}$) process and the continuum from the break-up process. Neutron fluxes in the continuum of quasi-monoenergetic neutron beams were almost half of the total neutron fluxes. The lowest neutron energies in the

TOF neutron measurements are limited by beam frequencies at each accelerator. The NIRS neutron energy spectra were measured with high cut-off energies, 15 and 35 MeV, for the 40 and 80 MeV p-Li neutron spectra, respectively, due to short beam intervals without beam chopping in the NIRS cyclotron.
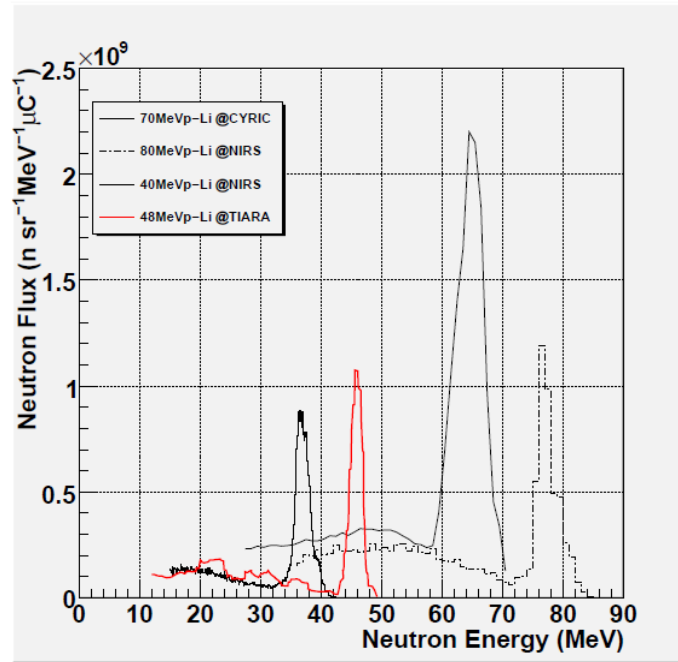

Fig. 3.1.4.4 Quasi-monoenergetic neutron energy spectra produced by the bombardment with 40, 48, 70 and 80 MeV protons onto thin lithium targets at NIRS, TIARA (Baba et al. 1999) and CYRIC (Baba 2006).

Table 3.1.4.1 Characteristics of quasi-monoenergetic neutron beams used in measurements of response functions at NIRS, TIARA and CYRIC neutron irradiation facilities.

Reaction	40 MeV p-Li	48 MeV p-Li	70 MeV p-Li	80 MeV p-Li
Peak Energy	36.9 MeV	46.0 MeV	64.9 MeV	77.1 MeV
Peak Width in FWHM	2.4 MeV	2.5 MeV	6.1 MeV	3.7 MeV
Facility	NIRS	TIARA	CYRIC	NIRS

The absolute neutron flux measurement was done at the CYRIC neutron beams with high

accuracy. The angular neutron response functions were measured by rotating the neutron detector from 0 to 180 degrees with respect to the neutron beams since neutrons are incident to the detector from all directions in the experimental jet flights. The acquired signal waveform was analyzed later in a laboratory. Light outputs from the detector were calibrated using photon sources of ^{137}Cs, ^{57}Mn, ^{60}Co, ^{22}Na, and 4.4 MeV photons from ^{241}Am-Be, and cosmic ray muons that were transmitted through the scintillator and created a 22 MeVee peak in light output.

The measured neutron response functions for the quasi-monoenergetic neutrons from the 70 MeV p-Li reaction were compared with the calculation in absolute values as shown in Fig. 3.1.4.5. In order to compare the shape of the response functions between the calculations and experiments, the measured response functions were normalized to the calculated results around the recoil-proton edges, which were calculated with high accuracy, within 5%. Good agreement was seen between the experimental and calculated absolute values, except at 90 degrees.
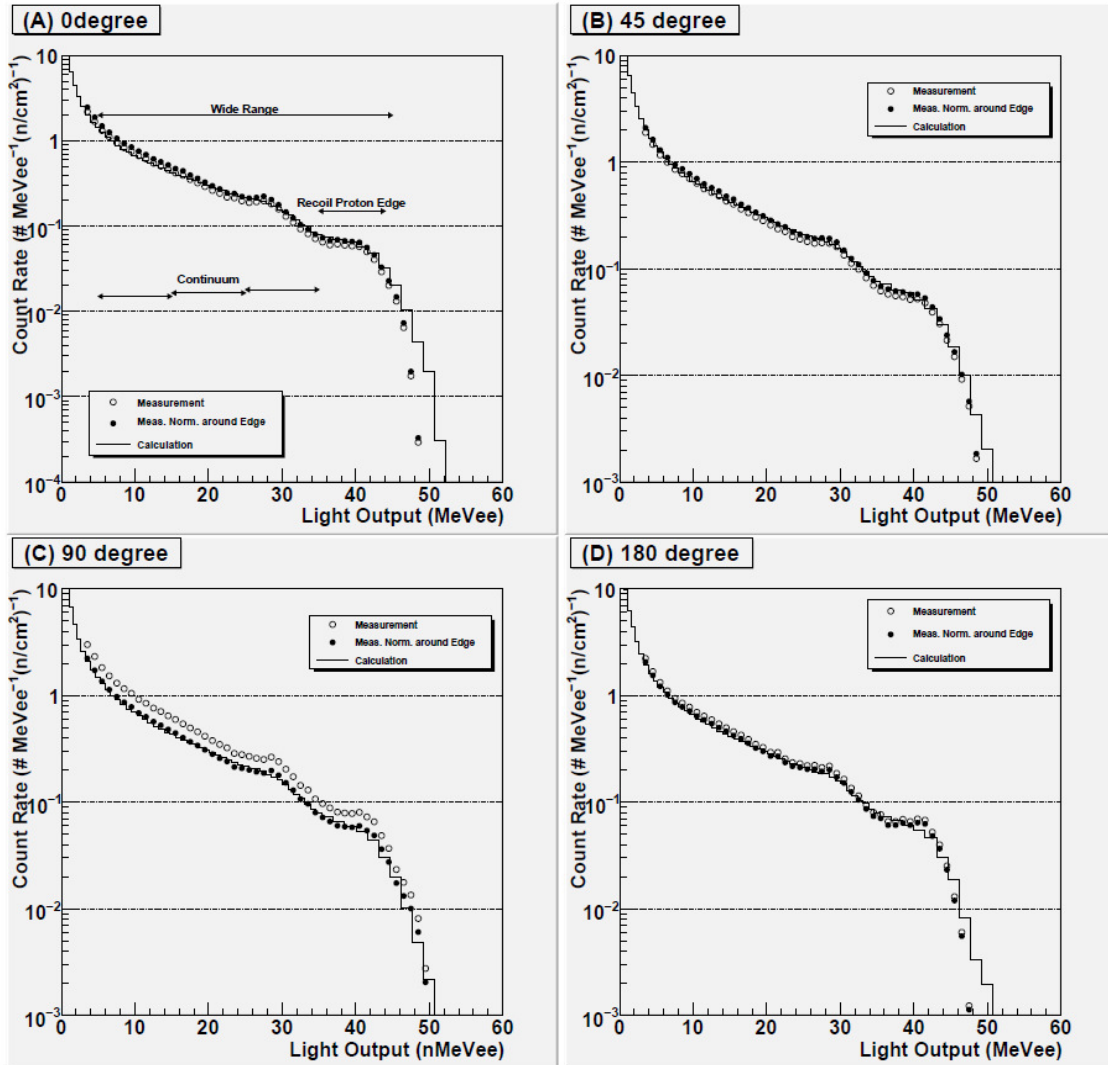
Fig. 3.1.4.5 Comparison of calculated and measured neutron response functions of quasi-monoenergetic neutrons from 70 MeV p-Li reaction for four incident angles: i.e., (A) 0, (B) 45, (C) 90 and (D) 180 degrees with respect to the cylindrical detector axis. Open circles and thin solid lines show the measured and calculated response functions in absolute values, respectively. Filled circles show the measurement normalized to the calculation around the recoil-proton edges, indicated with arrows in (A).

The ratios of calculated to measured response functions (C/E) are shown in Table 3.1.4.2. This work showed that the response functions agreed with the measurements, within 12% in absolute values, except at 90 degrees. The difference between the calculations and measurements could be induced from the dark current in the measurement of beam current and the neutron energy spectrum measured for the CYRIC neutron beam.

Table 3.1.4.2 Ratios of calculated to measured response functions (C/E) in absolute values for 70 MeV p-Li neutrons around recoil proton edges, wide light-output ranges and continuous regions indicated by arrows in Fig. 3.1.4.5 (A) at 0, 45, 90 and 180 degree incidences of neutrons to the detector axis.

Region in MeVee	0 degree	45 degree	90 degree	180 degree
Quasi-monoenergetic neutrons from 70 MeV p-Li reaction at CYRIC				
proton edge (in absolute value)	1.12	1.11	0.75	0.92
wide range, 5-45 MeVee (in absolute value)	1.00	1.05	0.72	0.91
5-15 MeVee (in relative value)	0.85	0.92	0.94	0.98
15-25	0.96	1.00	1.04	1.03
25-35	0.92	0.94	0.96	0.94
from 80 MeV p-Li reaction at NIRS				
10-20 MeVee (in relative value)	0.71	0.69	0.70	–
20-30	0.88	0.87	0.90	–
30-40	0.93	0.93	0.98	–
from 40 MeV p-Li reaction at NIRS				
8-13 MeVee (in relative vlaue)	0.88	0.80	0.88	–
13-18	1.25	1.01	1.10	–
18-23	1.12	1.04	1.02	–
from 48 MeV p-Li reaction at TIARA				
4-9 MeVee (in relative value)	0.80	–	0.78	0.90
9-19	0.93	–	0.89	0.98
19-29	1.04	–	0.97	1.03

Response Matrices

Neutron and photon response matrices are required in order to measure the neutron and photon energy spectra over a wide energy range. From the thus-verified results of the calculated response functions, response matrices were created based on the MCNPX simulation (MCNPX

2005) using the anti-coincidence mode, considering the light-output correlations with particle energies, the uniformity of light collection and the energy resolution (Takada et al. 2010 latter). Fig. 3.1.4.6 shows the response matrices for neutrons up to 200 MeV.
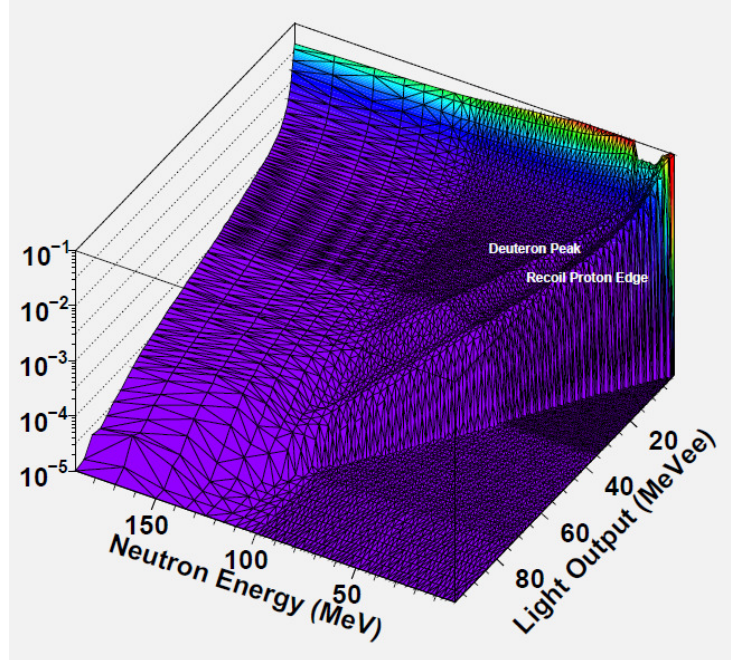

Fig. 3.4.1.6   Neutron response matrices created with the MCNPX code for the phoswich detector.

Light output

Particle light outputs were measured at the NIRS cyclotron by direct incidence of particles in the liquid scintillator (EJ-399). For the light-output measurements, a liquid-scintillator cell of 5.08 cm in diameter was produced to decrease the particle energy loss in the detector walls. The thicknesses of both the front and the side faces of this liquid scintillator cell were 0.5 mm. Light-output curves were obtained of protons up to 70 MeV, deuterons up to 50 MeV and helium ions up to 100 MeV. The measured proton light outputs were compared with the proton light-output function of the BC-501A liquid scintillator, as shown in Figure 3.1.4.7. The light outputs of the EJ-399-06 are a few percentage smaller than those of the BC-501A. The proton light-output function was obtained as:

$$L(MeVee) = 0.766 \times Ep - 2.89 \times (1-\exp(-0.187 \times Ep)) \qquad (1)$$

where L is light output and Ep is proton energy (MeV).

Scintillations created by neutrons in the phoswich detector are attenuated by the liquid scintillator. The light attenuation in the EJ-399-06 was measured by charged particle incidence on the side wall of the cell and resulted to be 1/10.5 (cm^{-1}). The light attenuation in the liquid scintillator consists of two components: one is the scintillation transmission directly to the PMT

window and the other is the reflection of scintillation at the front face of the detector. Scintillations created at a distance t from the rear face of the liquid scintillator are transmitted along a distance t and 2L-t for the former and the latter cases, respectively, where L is the liquid scintillator length. The attenuation curve was obtained by the formula:

$$f \; = \; a_1 \exp(-t/b) + a_2 \exp(-(2L-t)/b) \qquad\qquad (2)$$

where a_1 and a_2 are normalization factors and b is attenuation length in the EJ-399-06 liquid scintillator.

In the phoswich detector, a scintillation created in a space close to the front face of the liquid scintillator can be attenuated by 15% at its rear face. In order to confirm the measured light output of protons, light outputs of protons recoiled by 13, 38 and 66.5 MeV neutrons were also measured (Fig. 3.1.4.7). Light outputs of protons recoiled by neutrons agree with the light outputs measured with direct incident protons within the uncertainties given by the neutron energies and by the widths of the proton peaks.
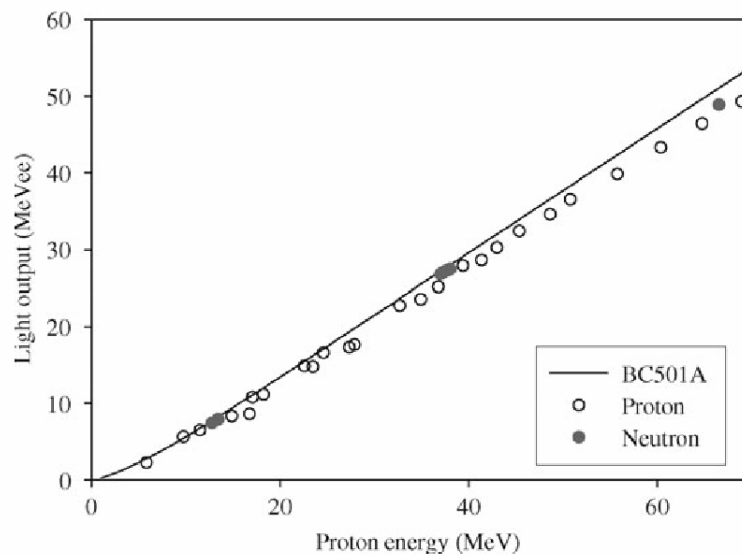

Fig.3.1.4.7 Light output functions of protons incident on the liquid scintillator directly (open circles), compared with protons recoiled by neutrons (closed circles) and light outputs of BC-501A liquid scintillator (solid line).

Simulation

The Monte Carlo N-Particle eXtended code (MCNPX), version 2.5.d. (MCNPX2005) was applied to simulate the neutron response functions. In the phoswich detector, protons were rejected from the neutron pulse heights. Part of the neutrons was also detected in the plastic scintillator. In neutron measurements, the phoswich detector identified neutron events detected

by the plastic scintillator as proton events. In the simulations, the events detected in the plastic scintillator had to be rejected from the neutron pulse heights. This was accomplished by applying the anticoincidence mode in the simulation scoring, where the events detected in both the plastic and liquid scintillators were thus rejected. The simulation geometry consisted of the liquid and plastic scintillators, the aluminum and acrylic covers and the acrylic light guide with their actual sizes, though no PMT was added in the detector configuration. Protons, deuterons, helium ions, electrons and gamma rays produced by neutrons in the detector configuration were transported up to 150 MeV with the neutron cross-section data library, LA150. Proton, deuteron and helium-ion pulse heights were obtained by scoring the events of charged particles detected only in the liquid scintillator and not in the plastic scintillator. The energies deposited in the liquid scintillator by each particle were converted to light outputs.

In order to study the angular dependence to neutrons, the detector responses were simulated for 70 MeV neutrons with different incident directions, from the front, the side, the back and the oblique angle of the detector. No difference between the calculated neutron responses was found at the different incidence directions accounted for. Therefore, all the response functions were calculated with neutrons impinging on the front face of the detector.

The detector response functions to neutrons up to 150 MeV were obtained by summing up the pulse heights of each particle, converted from deposited energies to light outputs, as shown in Figure 3.1.4.5. The shapes of calculated response functions agreed well with the measurements except for some discrepancies. Some events were found in the calculated pulse heights above the maximum proton energies, equal to the incident neutron energies. The events were eliminated from neutron responses. Because in the MCNPX code, neutrons are transported as non analog, the multiple protons produced by neutrons via the $C(n,2p)$ and other reactions are sampled independently from each other. Therefore, more energy than what went into the reaction can be obtained.

Data acquisition system

The pulse shapes of the output signals from the phoswich neutron detector were acquired directly. Several advantages are obtained by measuring signal shapes; acquire maximum amounts of information from the detector, separate pile-up signals at an off-line analysis and no adjustment of electrical circuits before measurements. Measured signals are analyzed off line to discriminate neutron events from photons and charged particles and obtain pulse heights. As shown in Figure 3.1.4.2, difference of signals on incident particles can be observed in low voltage of signals. To measure pulse shape and wide dynamic range of signal voltage, a portable data acquisition unit is made in this study as shown in Figure 3.1.4.8. Signals from the phoswich detector can be recorded using the data acquisition unit. A flash ADC with 500 MHz sampling

rate and 12 bits dynamic range is incorporated in the unit. The data acquisition unit measures 0 to 5 V signals from -20 to 400 ns with the maximum waveform storing speed at 350 signals s^{-1} (Figure 3.1.4.9). Signal voltages of 2 ns time period are stored in the onboard memory and then transferred to a personal computer via the USB2.0. Low waveform storing speed would lose detected events; however, 10 MHz event trigger corrects the number of true events. We think that its sampling rates can follow particle measurements in the International Space Station.
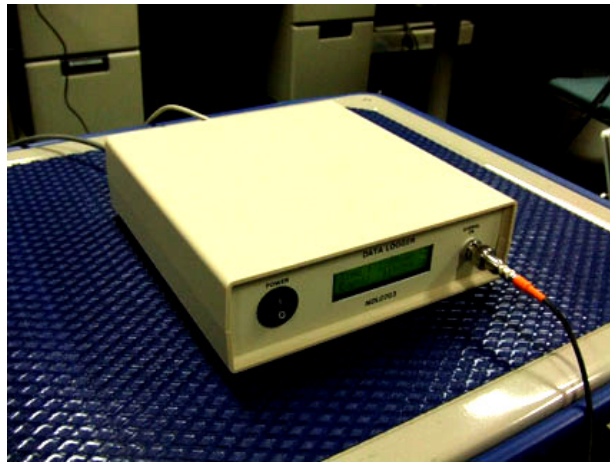

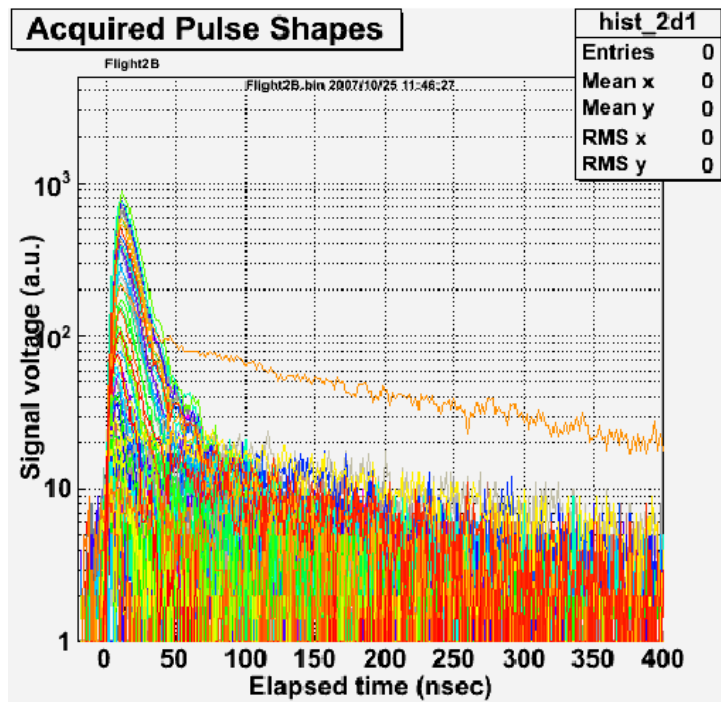Fig.3.1.4.8   A photo of the data acquisition unit NDL0703 which has a flash ADC with 500 MHz sampling ability.

Fig.3.1.4.9   Acquired signals from the phoswich neutron detector using the laptop data acquisition unit with 500 MHz and 12 bits flash ADC.

21

This data acquisition unit which is coupled with a phoswich detector, a small high voltage supply and a personal computer installed with data analyzing program (Fig. 3.1.4.10), has been named as "CREPAS" (Cosmic Radiation and Energetic Particle Analyzing System) by the authors.
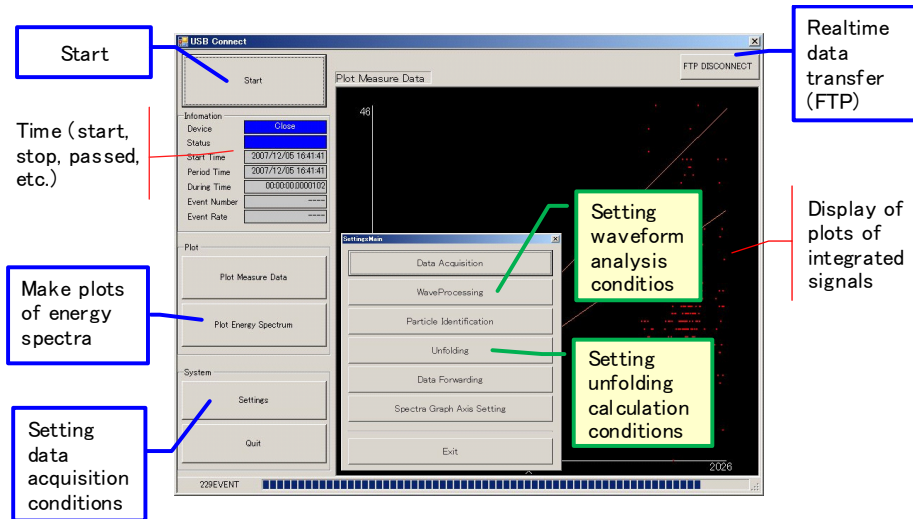

Fig.3.1.4.10　The data analyzing program developed for CREPAS.

Figure 3.1.4.11 shows the two-dimensional plots of signal integrals displayed on the CREPAS software for selected quasi-monoenergetic neutrons and monoenergetic protons supplied at particle accelerators in Japan; they are (a) 45 MeV neutrons at JAEA- TIARA and (b) ~ 230 MeV protons at NIRS-HIMAC. The X values of the figures are fast signal components (-20 to 100 ns from the trigger point) and Y values are slow components (150 to 400 ns) that come from the plastic scintillator. The voltage of photomultiplier was -1,200 V and the trigger level was -0.1 V in all the cases.   It is seen that the plots of high-energy neutrons within a specific area (lower part of the plot area) and, in comparison with the results of proton beams (Fig. 3.1.4.11b), we can expect that energetic cosmic-ray neutrons can be well discriminated from protons using this system.
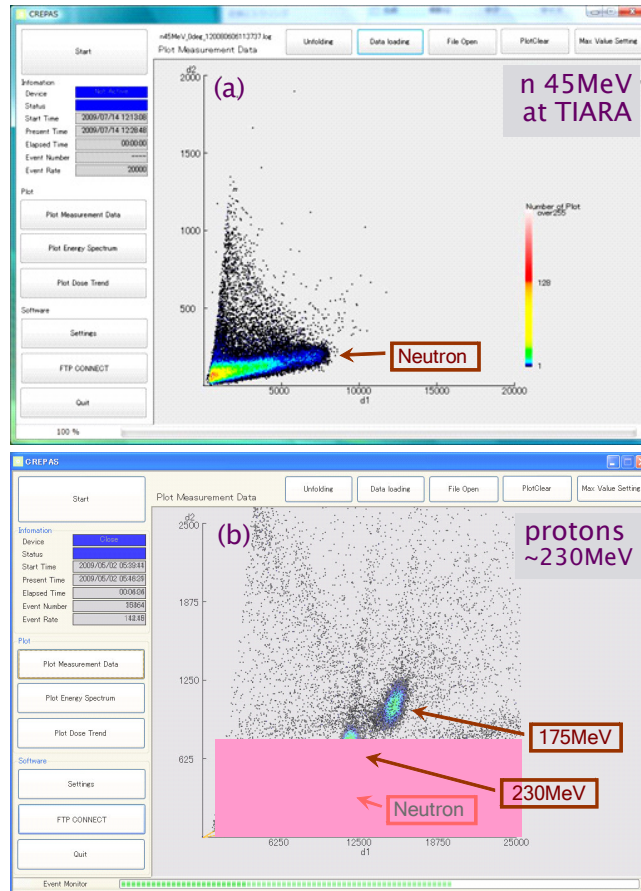
Fig.3.1.4.11   Two-dimensional plots displayed on the CREPAS software of fast versus slow signal integrals obtained for quasi-monoenergetic 45 MeV neutrons supplied at JAEA-TIARA (a) and monoenergetic ~ 230 MeV protons at NIRS-HIMAC (b).

3-2. Flight Conditions

The instruments were firmly fixed on to a rack and placed in a business jet aircraft (MU-300) as shown in Fig.3.2.1.   The aircraft departed from the Nagoya airport (35.3°N, 136.9°E) and flew six times along different routes near the Chubu area of the Honshu Island in Japan (Fig.3.2.2).   In this report, we focused on two representative routes as shown in Table 3.2.1.

The first run was a 96-min south-route flight on October 24, 2007, and the second run was a 140-min north-route flight on February 13, 2008.   The flying time at the highest altitude was 54 min at 9.1 km (30,000 ft) in the first run and 37 min at 11 km (36,000 ft) in the second run. Changes in aviation altitude were measured using a GPS and the recorded data were corrected to atmospheric pressure altitudes that were displayed on the monitor of a built-in altimeter. Temperature inside the aircraft was maintained at 20-25 °C and the cabin pressure at 0.8-1.0 atm.
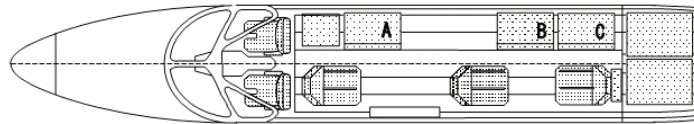
Fig.3.2.1 The external appearance (upper) and the cross view (lower) of the business jet
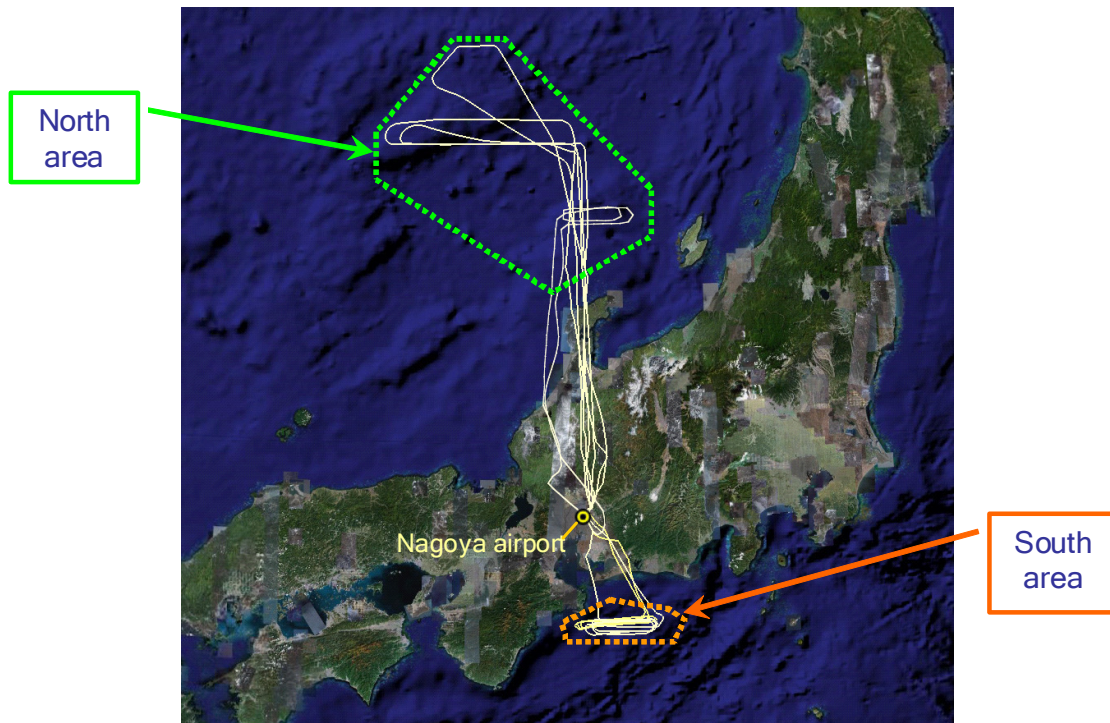aircraft MU-300.

Fig.3.2.2 Flight routes employed for the experiments from 2006 to 2008.

Table 3.2.1　Conditions of the representative flights chosen in this study.

No	Date	Cruising conditions		
		Altitude [km]	Latitude [deg.]	Time [min]
1	October 24th, 2007	9.1	34.0°N	54
2	February 13th, 2008	10.8	39.0°N	37

3-3. Radiation Model in the Atmosphere

Development of a model for estimating cosmic-ray spectra in the atmosphere is indispensable for estimating doses for each aircrew, since the doses depend on altitude, geomagnetic location and solar activity (referred to here as global conditions) along the flight routes in a complicated manner, and it is impractical to measure the doses for all flight conditions. A number of studies have been devoted to the construction of the model. For instances, Ziegler (1998) proposed an empirical formula for predicting the high energy neutron spectra. O'Brien et al. (1978) developed a deterministic code LUIN based on an analytical two-component solution of the Boltzmann transport equation. The code is capable of estimating the altitude dependences of aircrew doses and integrated neutron fluxes precisely, and is adopted in the route dose calculation code CARI-6 (FAA 2008). Several authors (Roesler et al. 1998; Ferrari et al. 2001; Clem et al. 2004) adopted a Monte Carlo particle transport code, FLUKA (Ferrari et al. 2005; Battistoni et al. 2007), for the calculation of the cosmic-ray propagation in the atmosphere. Their calculation methods were successful in reproducing the neutron spectra measured at high altitudes, and a similar model was employed in the European Program Package for the Calculation of Aviation Route Doses EPCARD (GSF 2008). However, the cosmic-ray neutron spectra depend not only on the atmospheric depth, cut off rigidity and solar modulation (referred to here as global conditions) but also the structure of the aircraft (Ferrari et al. 2004) and the water density around the point of interest (Roesler et al. 1998) (referred to here as local geometries) in an intricate manner, and none of the existing models are able to reproduce the measured neutron spectra at any location and time with satisfactory accuracy.

With these situations in mind, we have calculated the cosmic-ray spectra by performing Monte Carlo particle transport simulation in the atmosphere based on the Particle and Heavy Ion Transport code System PHITS (Iwase et al. 2002), utilizing the latest version of the nuclear data library JENDL-High-Energy File (JENDL/HE) (Fukahori et al. 2002; Watanabe et al. 2005).

In the simulation, cosmic-rays with charges up to 28 (Ni) were incident on the earth system represented by the concentric spherical shells, and the neutron spectra in each shell, i.e. a certain altitude range, were obtained. Based on a comprehensive analysis of the simulation results, we proposed analytical functions to predict the cosmic-ray neutron as well as proton, He ion, muon, electron, positron and photon spectra at any global condition at the altitudes below 20 km, considering the local geometry effect. The model was designated "PARMA":   PHITS based Analytical Radiation Model in the Atmosphere. The details of the simulation procedure together with the derivation procedure of PARMA were described in refs. (Sato and Niita 2006; Sato et al. 2008). Using PARMA, we have developed EXcel-based Program for Calculating Cosmic-ray Spectrum (EXPACS), which can calculate not only cosmic-ray spectra but also the corresponding effective dose and ambient dose equivalent for any locations in the world. The software has been opened for public from its web site (Sato et al. 2008).

As an example of the calculated results, the atmospheric neutron spectra at flight altitudes as well as ground level obtained from the PHITS simulation and PARMA are depicted in Figure 3.3.1, in comparison with the corresponding experimental data measured with the Bonner Ball Neutron Detectors (Goldhagen et al. 2004; Nakamura et al. 2005). It is evident from the graphs that the PHITS can reproduce the experimental data even at the ground level. Furthermore, PARMA is substantially superior to the PHITS simulation in reproducing experimental data at lower energies. This is because the local geometry effect on the spectra is precisely considered in the PARMA calculation, providing the water density in ground or the mass of aircraft to the functions. Comparison between the PARMA calculation and the DOSCONA   experimental data will be given in the next section.
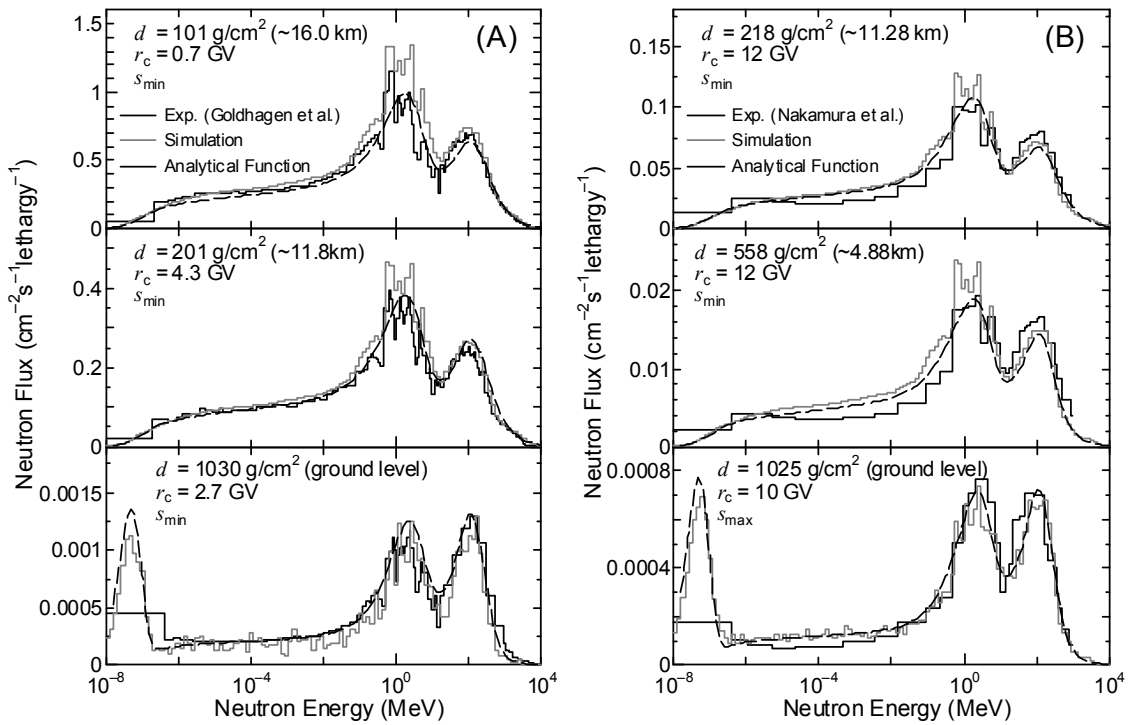
Fig.3.3.1. Calculated and experimental neutron spectra in the atmosphere for various global conditions. The panels (A) and (B) show the comparison with the data measured by Goldhagen et al. (2002) and Nakamura et al. (2008), respectively. The values of d, r_c and s are the atmospheric depth, the cut-off rigidity, and force-field potential respectively.

4. Results and Discussion

4-1. Experimental Results

4-1-1. Neutron Rem Monitors

Time-lapse changes in flight altitude and cumulative H*(10) values of three monitors are plotted in Fig.4.1.1.1 for the first flight and Fig.4.1.1.2 for the second one. As expected, the dose rate (degree of the slopes) corresponds well to flying altitudes; and a larger dose rate was observed at higher altitude with thinner atmosphere. The average H*(10) rates measured at the highest altitude during each flight are shown in Table 4.1.1.1. A large difference by a factor of 20 is found among the measured dose rates of these monitors. The order of the dose rate was PRESCILA > WENDI-II > NCN1 in both cases.

This difference is attributable to the difference in their response functions; the

27

^{252}Cf-normalized relative responses as a function of neutron energy are shown in Fig.4.1.1.3. The detection efficiency of the NCN1 drops sharply at energies greater than 15 MeV. In contrast, the WENDI-II maintains a relatively flat response for a higher energy range up to GeV. For the determination of responses to cosmic radiation, the relative efficiency of the NCN1 at the energies greater than 40 MeV and also that of the WENDI-II at more than 5 GeV are assumed to be constant (Fig. 4.1.1.3). The response of the PRESCILA seems to be flat up to around 100MeV according to our results of 65 MeV neutron exposure and calibration data recently published by Olsher and McLean (2008). Here, the relative response of the PRESCILA is assumed to be constant for energetic neutrons with tens of MeV as shown in Fig.4.1.1.3. Since cosmic neutrons contain the high energy components, such a difference in response functions is expected to significantly affect the monitor dose values.

In order to confirm this expectation, the measured neutron dose rates were compared to model calculations performed with the PHITS-based Analytical Radiation Model in the Atmosphere "PARMA" (Sato et al. 2008). The estimated H*(10) rates in the aircraft at the highest altitude were 0.75 μSv h^{-1} for the first flight (latitude: 34°N, altitude: 9.1 km and solar modulation potential: 407 MV) and 1.33 μSv h^{-1} for the second flight (latitude: 39°N, altitude: 11 km and solar modulation potential: 380 MV). Excellent agreement (<7% error) was seen in the values of the WENDI-II. The dose rate values of the NCN1 were lower by a factor of approximately two relative to the calculations; the values of the PRESCILA were very high by a factor of approximately 8.

In regard to the neutron dose distributions (Figs. 4.1.1.4 and 4.1.1.5) estimated with PARMA and response functions, the WENDI-II showed a nearly identical shape with the predicted H*(10) values. Estimated dose distribution of the NCN1 was much lower at energies greater than 20 MeV; however, the estimated values were about 60% of the observations. The response function of the NCN1 should be more thoroughly examined using monoenergetic neutrons produced from accelerated proton beams. The values of the PRESCILA were beyond the calculations at energies greater than 5 MeV; total doses were estimated to be twice as high as the calculations. The actual values, however, are notably lower than the measured ones. Such excessive response of the PRESCILA is attributable to the threshold level setting for n/γ discrimination, although the default setting was employed at this time. The contribution of directly incident cosmic protons can also be pointed out; they should produce identical pulses with those from neutrons in the ZnS scintillator of the PRESCILA. In order to quantify the effects of charged particles, we plan to examine the response of the PRESCILA to monoenergetic protons with a broad range of energy from MeV to GeV.

The effects of other components such as muons and pions are to be quantified experimentally in future studies. For this purpose, it is necessary to develop a novel radiation monitor that can

clearly distinguish and measure each different component of cosmic radiation in aircraft.
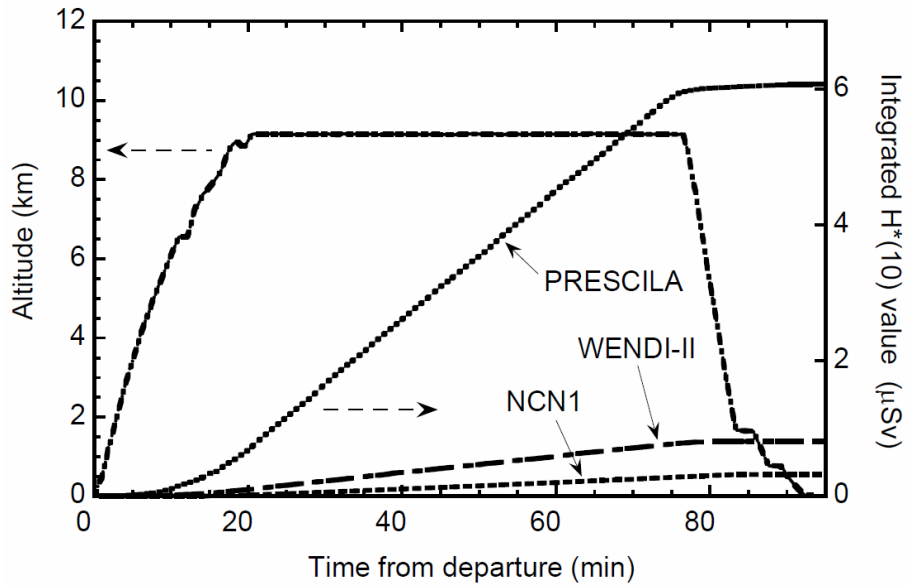

Fig. 4.1.1.1 Time-lapse changes in flying altitude and cumulative H*(10) values of three monitors during the first flight (Oct.24, 2007).
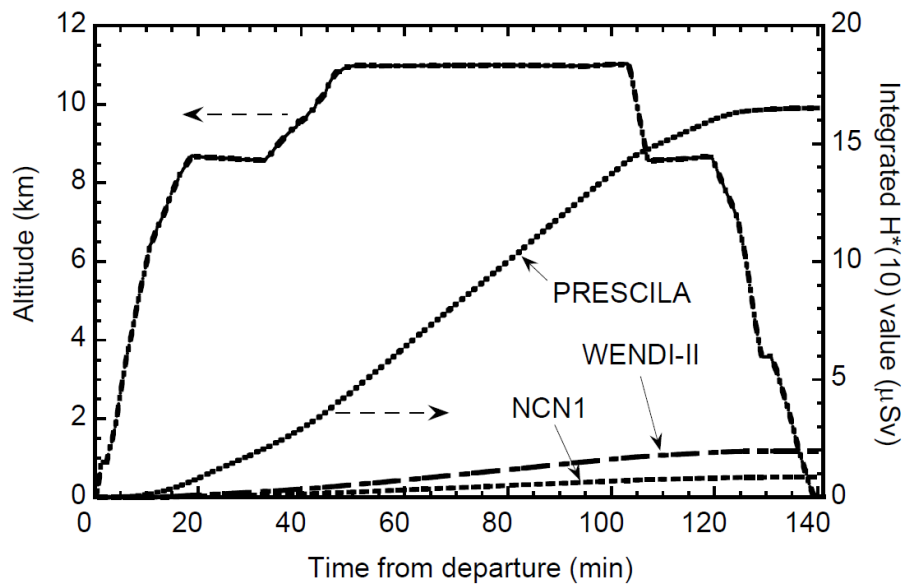

Fig. 4.1.1.2. Time-lapse changes in flying altitude and cumulative H*(10) values of three monitors during the second flight (Feb.13, 2008).

Table 4.1.1.1   Flight conditions and the neutron monitor values obtained at the highest altitude during two flights near Japan (about 137°E) on (1) Oct.24, 2007 and (2) Feb.13, 2008.

No.	Altitude [km]	Latitude [deg.]	Time [min]	Ambient dose equivalent rate [μSv h^{-1}]			
				NCN1	WENDI-II	PRESCILA	Model*
1	9.1	34.0°N	54	0.29+/-0.011	0.70+/-0.018	5.6+/-0.055	0.75
2	10.8	39.0°N	37	0.56+/-0.007	1.32+/-0.030	10.5+/-0.066	1.33

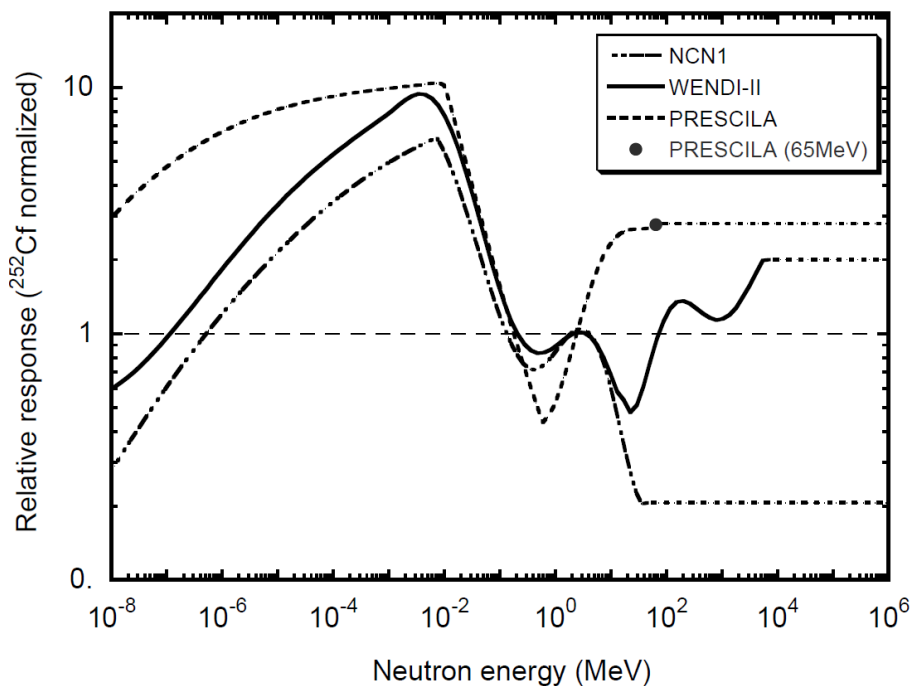* The PHITS-based Analytical Radiation Model in the Atmosphere PARMA.

Fig 4.1.1.3   Energy-response functions of the three neutron monitors; the relative responses of the NCN1 and the WENDI-II were calculated using the MCNPX code by Nakane et al. (2004) and Olsher et al. (2000), respectively; the responses in the high-energy region (more than 40 MeV for the NCN1 and more than 5 GeV for the WENDI-II) were assumed to be constant.   The response of the PRESCILA for energies less than 20 MeV was given by Olsher et al. (2004) and it was assumed to be constant for energies greater than 65 MeV according to the results using 65 MeV p-Li neutrons obtained at the cyclotron of Tohoku University and calibration data recently published by Olsher and
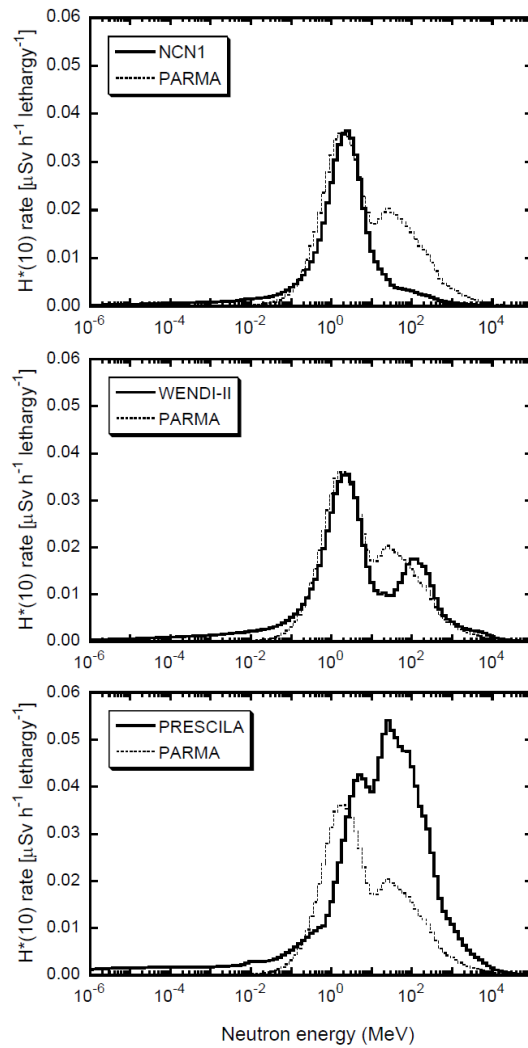
McLean (2008).

Fig 4.1.1.4 The neutron dose distribution estimated from the response functions of three monitors (upper: NCN1, middle: WENDI-II and lower: PRESCILA) at the highest altitude in the first flight (Oct.24, 2007); it is compared with that calculated with PARMA.
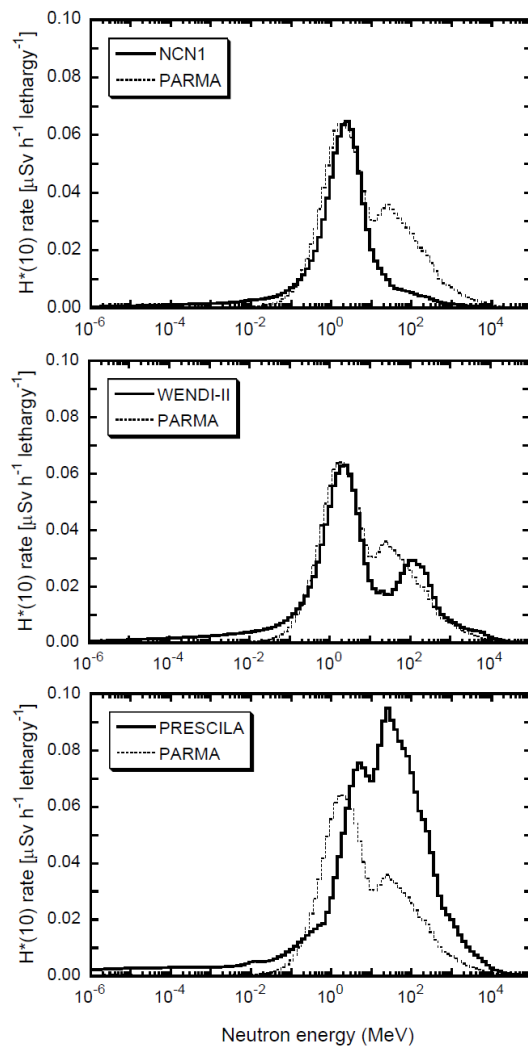
Fig 4.1.1.5 The neutron dose distribution estimated from the response functions of three monitors (upper: NCN1, middle: WENDI-II and lower: PRESCILA) at the highest altitude in the second flight (Feb.13, 2008); it is compared with that calculated with PARMA.

4-1-2. DARWIN

The dose rates measured with DARWIN at the flight experiment on March 2, 2007 are shown in Figure 4.1.2.1, in comparison with the corresponding data calculated by EXPACS. The shielding effect of the aircraft was considered in the EXPACS calculation. The time constant of the experimental data is approximately 5 seconds. The measured neutron dose rates shown in this graph are the corrected values. The measured photon+lepton dose rates represent the sum of the doses estimated from the photon and muon scintillations applying the G-function method, including the contribution from the miss-identified scintillations triggered by the electron and

positron incidences. The corresponding calculated values are the sum of the photon, muon, electron and positron dose rates. The altitudes of the aircraft recorded by GPS are also depicted in this graph.

Excellent agreement can be observed between the experimental and calculated data over the wide altitude range except for the photon+lepton dose rates near ground level. At the highest altitude (~10.4 km), the measured neutron and photon+lepton dose rates were 1.15 ± 0.006 and 0.76 ± 0.001 μSv h^{-1}, respectively, where the uncertainties were derived only from the statistical error were not included. The corresponding calculated data are 1.15 and 0.73 μSv h^{-1}, respectively. These agreements clearly indicate the applicability of DARWIN in monitoring doses in complex radiation fields.

The disagreement in the photon+lepton dose rates near ground level are attributed to the ignorance of the photon doses emitted from the earth in the EXPACS calculation. On the other hands, the measured neutron dose rates agree with the calculated data even during takeoff and landing. These two facts verify the capability of DARWIN in monitoring the small fluctuation of dose rates near the background level. This feature makes DARWIN useful in monitoring doses at surrounding environments of accelerator facilities, where the dose rates are generally close to the background level.
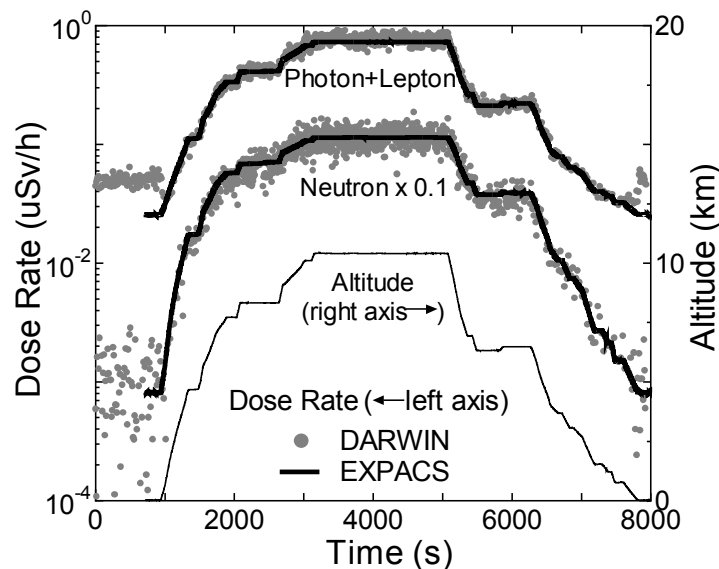

Fig.4.1.2.1. Dose rates measured with DARWIN at the flight experiment on March 2, 2007, in comparison with the corresponding data calculated by EXPACS.

4-1-3. BBND

Count Rates

The count rates of the BBND sensors (integrated counts per one minute) and the altitude of the aircraft are plotted in Fig.4.1.3.1 against the elapsed time from the BBND measurement start for the flights on (a) Oct. 24, 2007, (b) Oct. 25, 2007, (c) Feb. 13, 2008 and (d) Feb. 15, 2008, respectively. Figure 4.1.3.1(a) shows a result of the south route, and Figs.4.1.3.1(b)-(d) show results of the north routes. The tendencies toward increases or decreases in the aircraft's altitude accord very well with count rates of the BBND sensors. Because the relationship between the fluence rate of the cosmic-ray neutrons and the altitude is not linear and the contributions of the latitude and longitude changes to the neutron fluence rate could not be ignored, it is reasonable that the count rates and the altitude plot are not completely in agreement. In reference to the flight data obtained with the GPS, we picked up the BBND data for the unfolding process by selecting the period during which the aircraft maintained the prescribed altitude and latitude, and the change of longitude was quite small in the destination area. The period acquiring the data for the unfolding process of each flight is shown also in Fig. 4.1.3.1.

Unfolded spectra

Figure 4.1.3.2 shows a comparison of the measured unfolded spectra at 9.2 km altitude and N 34° latitude on Oct. 24, 2007, and at 10.8 km altitude and N 39° latitude on Feb. 13, 2008, and the spectrum measured by Nakamura et al. with the Bonner ball at 11.28 km altitude and the latitude near N 34.7° on Feb. 27, 1985 (Nakamura et al. 1987). The two measured spectra of the present work shown in Fig. 4.1.3.2 were chosen to match the altitude and the geographical latitude to those of Nakamura et al. as closely as possible for comparison. Except for a trivial bump at 1 eV and a pit at 4 MeV in the spectrum of Nakamura et al., the shapes of three spectra agreed well (Fig. 4.1.3.2). Taking into account that the cosmic-ray neutron fluence rate generally increases with the altitude and the latitude, it can be said that the relationship of the three spectra in magnitude is reasonable.
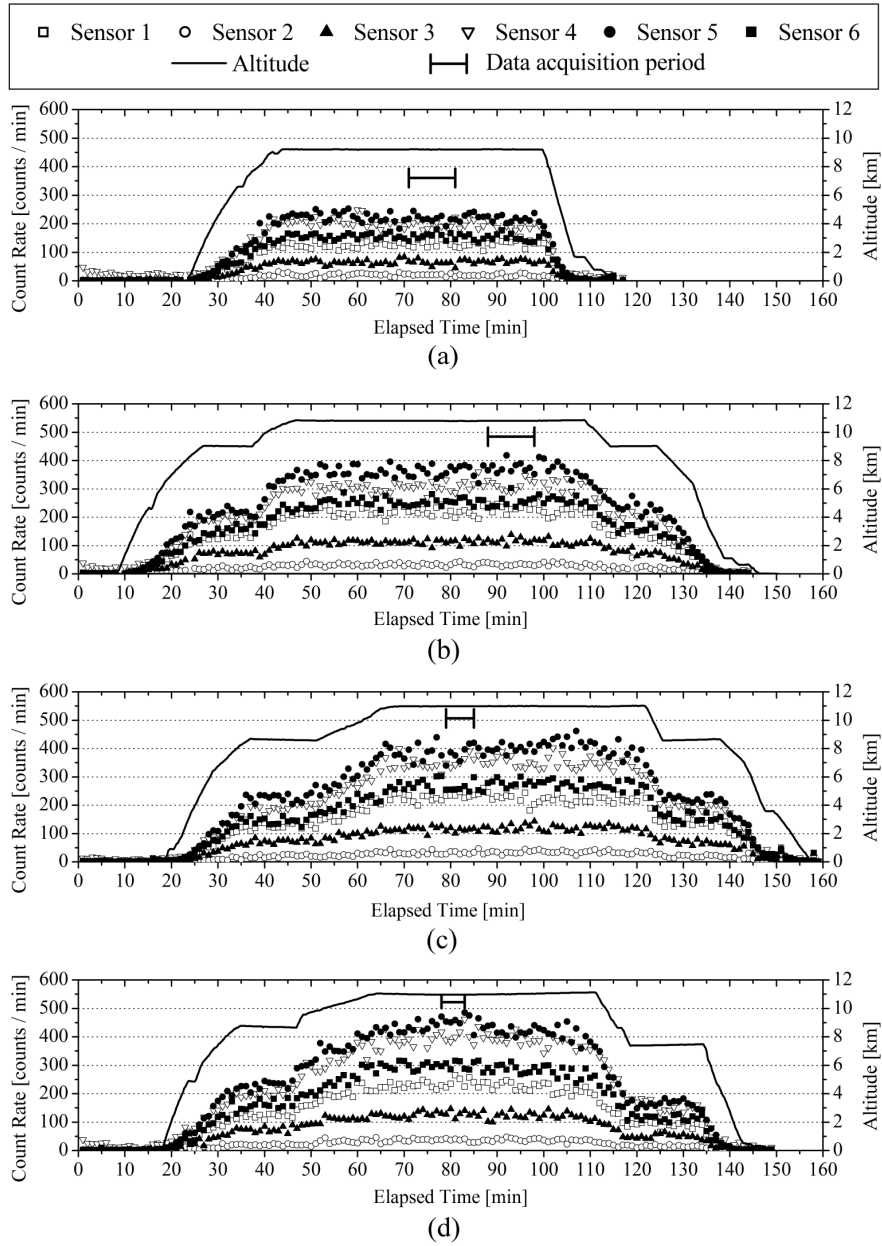
Fig. 4.1.3.1 Count rates of BBND sensors with the altitude change for (a) the south route flight on Oct. 24, 2007, (b) the North route flight on Oct. 25, 2007, (c) the North route flight on Feb. 13, 2008, and (d) the North route flight on Feb. 15, 2008.
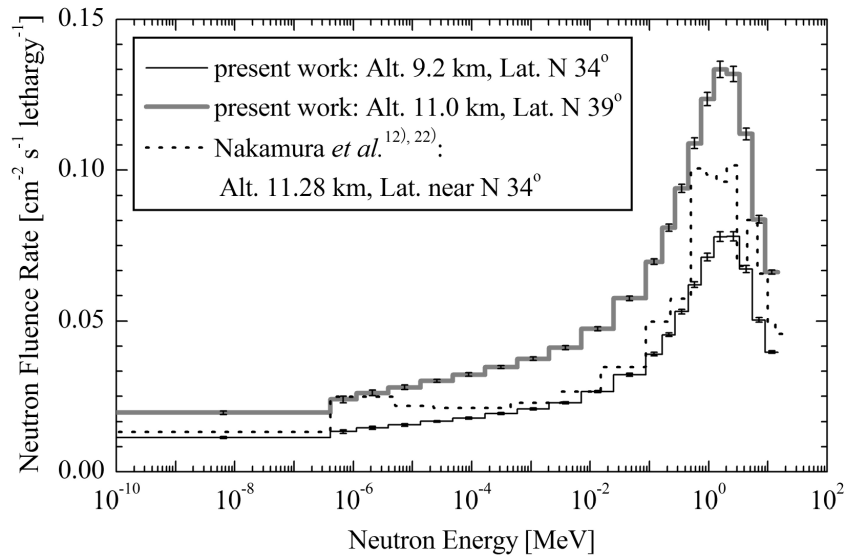
Fig. 4.1.3.2   Comparison of the measured unfolded spectra for present work and that
of Nakamura et al. (1987; 2004), both of which were measured with
Bonner ball in aircraft over Japan.

4-1-4. Phoswich Detector / CREPAS

Our measured neutron energy spectra from the flight experiment data, (A) in n cm^{-2} MeV^{-1} s^{-1} and (B) in n cm^{-2} s^{-1}, are plotted with error bars in Fig. 4.1.4.1 from 7 to 180 MeV at the aviation altitude (249 g/cm^2 atmospheric depth, 10.2 GV vertical cut-off rigidity) and a heliocentric potential of 312 MV. This energy spectrum was obtained by the unfolding method using the FERDOU code (Shin et al. 1981) with the neutron response matrix given by the authors, as seen in Fig. 3.4.1.6.   The energy spectrum (B) is equivalent to the lethargy spectrum. Our result shows a large, sharp neutron peak around 70 MeV and a lower-energy peak of 12 MeV.
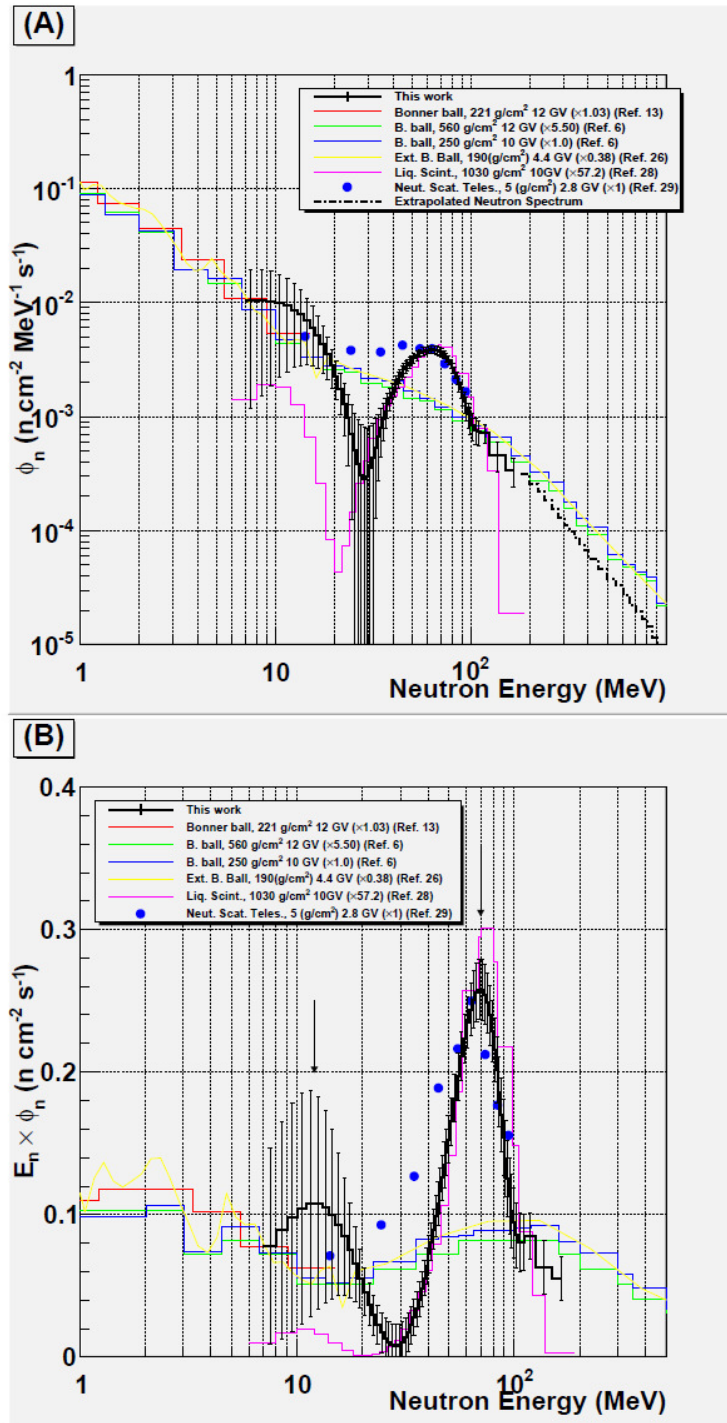
Fig. 4.1.4.1   Measured neutron energy spectrum at an altitude of 10.8 km
(atmospheric depth of 249 g/cm^2) and geographical latitude of 39°N
(vertical cut-off rigidity: 10.2 GV) on February 13, 2008 (heliocentric
potential: 312 MV (FAA 2009)). Our results are compared with other
measurements, normalized at our measured location, using an extended

Bonner ball (Goldhagen et al.2004), a Bonner ball (Nakamura et al. 2004; Yajima et al. 2010), an organic liquid scintillator on the ground (Nakamura et al. 2005), and a double-scatter neutron telescope at the top of the atmosphere (Preszler et al. 1974). (A) and (B) show the neutron flux and the flux multiplied by the neutron energy (i.e., the lethargy spectrum), respectively.   Our measured neutron spectrum, plotted as a dotted line in (A), is extrapolated smoothly.

At aviation altitudes, various Bonner ball experiments have provided a neutron energy spectrum (Fig. 4.1.3.2.). Nakamura et al.(2004) measured neutron energy spectra using a Bonner ball at atmospheric depths of 221 and 560 g/cm^2 (B.ball-1 and B.ball-2, respectively). Their measurements were conducted around Japan, close to our location, and their neutron energy spectra were obtained up to 1 GeV. Yajima et al.(2010) also measured the neutron energy spectrum using a Bonner ball (red line) on the same flight as our measurement, but their maximum energy was 20 MeV because their Bonner ball had low sensitivity to neutrons at energies greater than 20 MeV.   Goldhagen et al.(2004) measured the neutron energy spectrum using an extended Bonner ball (Ext. B. ball) incorporating heavy metal layers to improve the sensitivity to neutrons at energies greater than 20 MeV at an atmospheric depth of 201 g/cm^2 in the USA (4.4 GV vertical cut-off rigidity). Their neutron spectrum extended above 1 GeV. To compare these measurements with those of this study, their measured spectra were normalized at our measured locations, 249 g/cm^2 in atmospheric depth and geographical latitude 39°N, by correcting for neutron attenuation in air, considering the cut-off rigidity. Gordon et al.(2004) reported an analytical model of cosmic-ray neutron flux from the ground to 3.5-km altitude considering the vertical cut-off rigidity.   The attenuation length in air is reported to be 165 g/cm^2 for neutrons at energies above 20 MeV in Japan, which is obtained from the neutron flux from the ground to an altitude of 11.3 km.   The normalized factors are denoted in parentheses in the legends in Fig. 4.1.4.1.

In Fig. 4.1.4.1(B), three Bonner ball neutron spectra show a broad peak around 100 MeV with almost the same peak height. The widths of the peaks in our results and the Bonner ball results differ greatly. This is because of the energy resolutions of the detectors: the phoswich detector has 12 to 13% energy resolution in FWHM for 80 MeV neutrons, and the energy resolution of the Bonner ball is much worse in this high-energy region.

Table 4.1.4.1 Measured neutron fluxes compared with other measurements and calculations integrated within several neutron energy regions. Numbers in parentheses indicate the flux ratios of each result to our measured result. The last line shows the flux ratios considering the extrapolated neutron spectrum in our result.

Flux in neutrons cm^{-2} s^{-1}	This study	Ext. B. Ball[a][26]	B.Ball[b]-1[28]	B.Ball-2[28]
7−180 MeV	0.27 ± 0.019 (1.0)	0.25 (0.91)	0.22 (0.80)	0.24 (0.88)
30−100 MeV (peak)	0.15 ± 0.0028 (1.0)	0.11 (0.73)	0.09 (0.60)	0.10 (0.67)
7 MeV −	0.27 (1.0)	0.31 (1.15)	0.30 (1.11)	0.32 (1.19)
over 7 MeV + Ext. Spec.[c]	0.27+0.05 (1.0)	— (0.96)	— (0.93)	— (0.99)
	Liq. scint.[28]	LUIN2000[19]	EXPACS[23, 24]	RMC[31]
	0.23 (0.84)	0.45 (1.64)	0.27 (0.99)	0.25 (0.91)
	0.19 (1.27)	0.15 (1.00)	0.11 (0.73)	0.10 (0.67)
	0.23 (0.85)	0.57 (2.11)	0.39 (1.44)	0.35 (1.3)
	— (0.71)	— (1.76)	— (1.20)	— (1.08)

[a] Ext. B. Ball means external Bonner ball.

[b] B. Ball means Bonner ball.

[c] Ext. Spec means extrapolated neutron spectrum.

To confirm the accuracy of our measured neutron spectrum, our results and the other Bonner ball results are presented in Table 4.1.4.1 in our measured energy region, 7 to 180 MeV, and our peak energy region, 30 to 100 MeV. Our results are 15 to 40% larger than the Bonner ball measurements because of different neutron peak widths in our peak energy region from 30 to 100 MeV. The neutron fluxes from 7 MeV to 1 GeV are compared in the fourth line. As our maximum neutron energy and that of other Bonner ball observations were 180 MeV and 2 GeV, respectively, our neutron energy spectrum from 180 MeV to 2 GeV was obtained by extrapolating smoothly based on our results in the energy range from 100 to 180 MeV, shown as a dotted line in Fig. 4.1.4.1(A). The flux ratios of each result to our result plus this extrapolated flux, 0.05 neutrons cm^{-2} s^{-1} , are shown in the fifth line of Table 4.1.4.1. Our neutron fluxes above 7 MeV without considering this extrapolated neutron flux are 20% larger than the Bonner ball fluxes; when this extrapolated neutron flux is considered, our measured fluxes agree well with the Bonner ball fluxes within 7%, which is within the measurement uncertainties. This

confirms that our measured neutron fluxes are quite reasonable.

Besides the Bonner ball measurements, results from two experimental studies with high energy resolution are plotted in Fig. 4.1.4.1. One is the neutron spectrum measured with an NE213 organic liquid scintillator on the ground at Sendai (atmospheric depth of 1013 g/cm^2 and vertical cut-off rigidity of 10.4 GV) by Nakamura et al.(2005) (pink line), and the other is the neutron spectrum measured with a double-scatter neutron telescope at the top of the atmosphere (5 g/cm^2 altitude with a cut-off rigidity of 2.8 GV) by Preszler et al. (1974) (solid blue circles). The former is plotted by normalizing at our measured altitude using an attenuation length of 165 g/cm^2 (2005) and the latter is given in relative values for comparison to the neutron spectra. Both spectra show a sharp peak around 70 MeV. The peak can be demonstrated to result from the good energy resolution of these two detectors. The neutron energy spectra differ below the large peak around 70 MeV. The lower neutron flux below 30 MeV on the ground is found to be 20% of our neutron flux at the 249 g/cm^2 flight altitude, which could be caused by the difference in neutron attenuation. The attenuation lengths over 10 and 20 MeV are reported to be 155 (Gordon et al. 2004) and 165 (Nakamura et al. 2005) g/cm^2 , respectively.

This smaller attenuation length results in a neutron flux on the ground that is smaller by 26%. The smaller neutron flux below 30 MeV on the ground is found to be reasonable, although the difference in neutron energy spectra below 50 MeV between the phoswich detector and the double-scatter neutron detector cannot be explained. The neutron fluxes in several energy ranges with the liquid scintillator measurement are also shown in Table 4.1.4.1. The peak neutron fluxes from 30 to 100 MeV of our results and the liquid scintillator measurements agree within 27%. The Bonner ball measurements do not yield the sharp neutron peak because of the poor energy resolution, whereas the liquid scintillator and the double-scatter neutron telescope indicate sharp peaks around 70 MeV on the ground and at almost the top of atmosphere (5 g/cm^2 altitude), respectively. Because a large neutron peak around 70 MeV can be seen both at the top of the atmosphere and on the ground, the neutron peak around 70 MeV in our flight experiment is reasonable, which implies neutron propagation from the top of the atmosphere down to the ground.

4-2. Comparison with Model Simulations

4-2-1. Low to middle energy neutrons

The measured and calculated cosmic-ray neutron energy spectra are shown as neutrons cm^{-2} s^{-1} per unit lethargy in Fig. 4.2.1.1 for the measurement flight (a) at the altitude of 9.2 km and latitude of N 34° on Oct. 24, 2007, (b) at the altitude of 10.8 km and latitude of N 39° on Oct. 25, 2007, (c) at the altitude of 11.0 km and latitude of N 39° on Feb. 13, 2008, and (d) at the

altitude of 11.0 km and latitude of N 40° on Feb. 15, 2008, respectively. The conditions of the data acquisition for the unfolding process corresponding to Fig. 4.2.1.1 are presented in Table 4.2.1.1. The measured spectra (the solid histograms) were unfolded using MAXED, and the calculated spectra in ideal atmosphere (the solid lines) and considering the shielding effect in the aircraft (the dotted lines) were obtained using PARMA performed on the EXPACS version 2.13 (2008).   All the measured and calculated spectra in Fig. 4.2.1.1 have a peak around 1 MeV, and these accord with the past measured and calculated data (Goldhagen et al. 2004; Nakamura et al. 1987; Sato and Niita 2006).

The calculated spectra agree well with the measured results for the spectrum shape in Fig. 4.2.1.1. However, the calculations in ideal atmosphere exceed the measurements at the peak in magnitude by about 24% in Figs. 4.2.1.1(a)-(c), and about 16% in Fig. 4.2.1.1(d). This discrepancy is considered to reflect a shielding effect by the structures of the aircraft, qualitatively. That is, the body of the aircraft, various apparatuses installed in the cabin, and the humans (the pilots and the observers) aboard played a role in the dispersion and scattering of the cosmic rays and caused a reduction of the neutron fluence rate in the aircraft compared to that in ideal atmosphere. Ferrari et al. have developed an aircraft mathematical model and investigated the influence of aircraft shielding on cosmic rays (Ferrari et al. 2004). They stated that the neutron fluence rate in an aircraft can be reduced, especially at low energies, and estimated that the reduction would be about 56% at the seat of a typical passenger for the energy below 10 MeV under the condition of the aircraft carrying 278 passengers, baggage, cargo and fuel. Their argument cannot simply be applied to our findings in the present study because their model corresponds to a relatively large civil aircraft, whereas our chartered aircraft (MU-300) was a small business jet. However, we note that the influence of the reduction on the fluence rate in Fig. 4.2.1.1(d) was less than those in Figs. 4.2.1.1(a)-(c) because of all the observers aboard having been slender at the measurement for Fig. 4.2.1.1(d) compared to the other measurements for Fig. 4.2.1.1(a)-(c).

As mentioned before, we can estimate the neutron spectra inside an aircraft by PARMA, providing local effect parameters signifying the influence of the shielding effect with the model. See the spectra calculated by PARMA considering the shielding effect in the aircraft (the dotted lines) shown in Fig. 4.2.1.1 again. The local effect parameters that must be provided with the model are the location and the mass of the aircraft, and we set the parameters in order to reproduce our experimental data. The parameters we employed were not based on the real configuration, but according to Sato et al. (2008), the local effect parameters were introduced in PARMA only to express the magnitude of the influence of surrounding materials on the neutron spectra, and need not be realistic. Unfortunately, it is impossible to quantitatively argue the shielding effect in the aircraft based on the present results, using the current version of PARMA,

and the quantitative treatment of the shielding effect in the aircraft on the cosmic-ray neutron spectrum is being examined now. It is a problem to solve in the future, but we hope that the accuracy and usefulness of the calculation code PARMA will be improved when this problem is solved.

The energy spectrum obtained using unfolding procedure with Bonner-ball measurements is very sensitive to the default spectrum. Thus, we tried to examine the variability of unfolding results on the default spectrum.

Figure 4.2.1.2 shows cosmic-ray neutron spectra over a wide range of energy as neutrons cm^{-2} s^{-1} MeV^{-1} at 11.8 km altitude (200 g cm^{-2} in atmospheric depth) calculated by Armstrong et al. (Armstrong 1973) and measured by Hess et al. (1959) and at 11.28 km altitude measured by Nakamura et al. (Nakamura et al. 1987: 2005). The spectrum of atmospheric cosmic-ray neutrons has almost E^{-n} energy dependence, where E is the neutron energy and n is a positive number. In reference to the cosmic-ray neutron spectra in Fig. 4.2.1.2, n is roughly found for two energy ranges: 1 for the range from 1 eV to 10 MeV and 1.3 for the range from 10 MeV to 1 GeV. The functions proportional to E^{-1} and $E^{-1.3}$ are also shown in Fig. 4.2.1.2. We selected three testing default spectra; two of them were E^{-1} and $E^{-1.3}$ type functions, as those are monotones with no bump structure around 1 MeV, and the other was a spectrum calculated with PARMA having a peak around 1 MeV, as shown in Fig. 4.2.1.1. Then, using these default spectra, we performed MAXED unfolding tests for the BBND data at the altitude of 11.0 km and the latitude of N 39° measured on Feb. 13, 2008. The trial unfolded neutron spectra using the default spectra proportional to E^{-1} and $E^{-1.3}$ and determined by the PARMA calculation are shown in Fig. 4.2.1.3. We observed that the peak around 1 MeV appeared in all of the unfolded spectra. Therefore, we conclude that the characteristic of the unfolded measured spectra in Fig. 4.2.1.1 of having a peak around 1 MeV is not simply an inheritance from that of the default spectrum with the calculation. The unfolded spectrum for the default spectrum proportional to $E^{-1.3}$ differs rather from those of the others. In contrast, the unfolded spectra for the default spectra proportional to E^{-1} and with the calculation are very similar to one another. This shows that the E^{-1} function is a reasonable default spectrum for the energy range concerned in this work. The spectrum calculated with PARMA is a more appropriate default spectrum compared to the function proportional to E^{-1} because it reproduces the unfolded spectrum both in shape and magnitude as shown in Fig. 4.2.1.1. Thus, we conclude that the present BBND measurements with the MAXED unfolding process using the default spectrum calculated with PARMA have certain reliability.
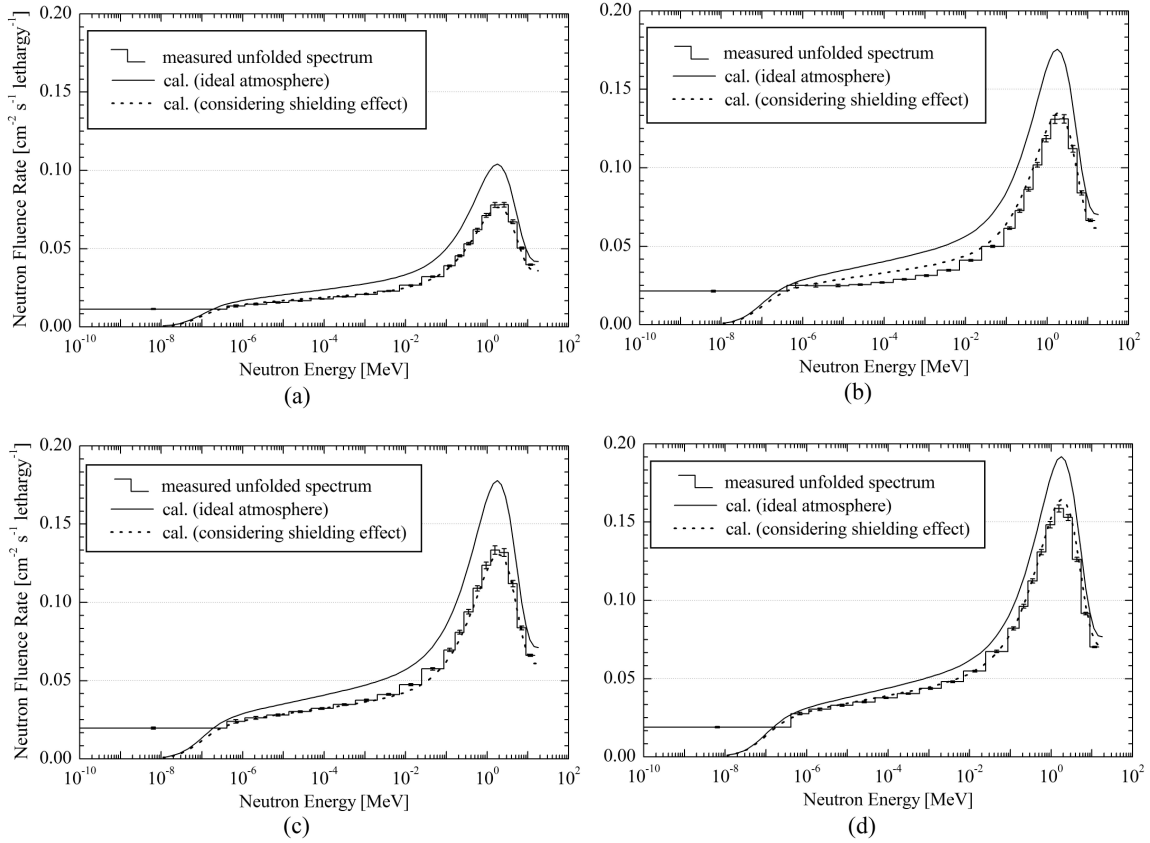
Fig. 4.2.1.1   Measured and calculated cosmic-ray neutron energy spectra (a) at an altitude
of 9.2 km and a latitude of N 34° for the flight on Oct. 24, 2007, (b) at an altitude of
10.8 km and a latitude of N 39° for the flight on Oct. 25, 2007, (c) at an altitude of
11.0 km and a latitude of N 39° for the flight on Feb. 13, 2008, and (d) at an altitude
of 11.0 km and a latitude of N 40° for the flight on Feb. 15, 2008.

Table 4.2.1.1   Data acquisition conditions for the unfolding process.

| Date of flight | Route | Altitude in the destination area | Geographical location | | Acquisition period | Corresponding fig. num. |
			Latitude in the destination area	Longitude in the destination area		
Oct. 24, 2007	South	9.2 km	N 34°	near E 137°	600 s	Fig. 8(a)
Oct. 25, 2007	North	10.8 km	N 39°	near E 135°	600 s	Fig. 8(b)
Feb. 13, 2008	North	11.0 km	N 39°	near E 135°	360 s	Fig. 8(c)
Feb. 15, 2008	North	11.0 km	N 40°	near E 135°	300 s	Fig. 8(d)
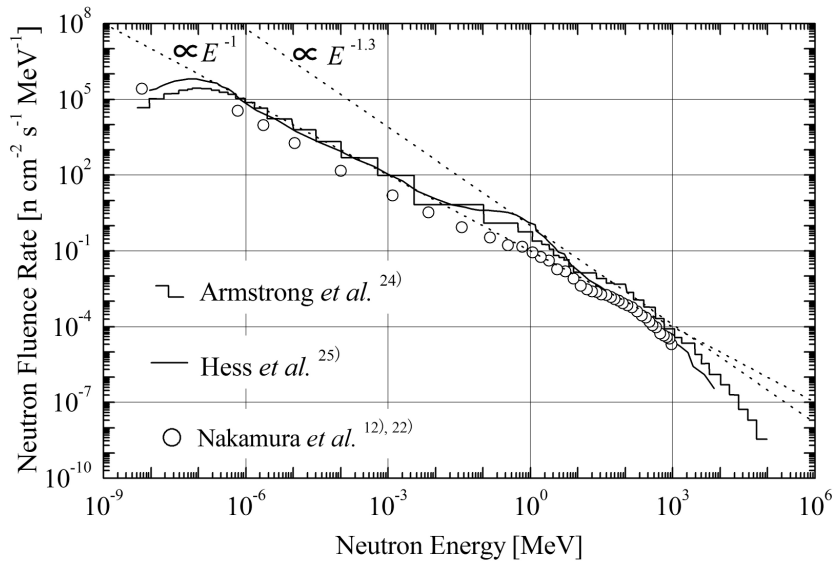
Fig. 4.2.1.2 Cosmic-ray neutron spectra over a wide range of energy at 11.8 km altitude calculated by Armstrong et al. (1973) and measured by Hess et al. (1959) and at 11.28 km altitude measured by Nakamura et al. (1987; 2005) with the functions proportional to E^{-1} and $E^{-1.3}$.
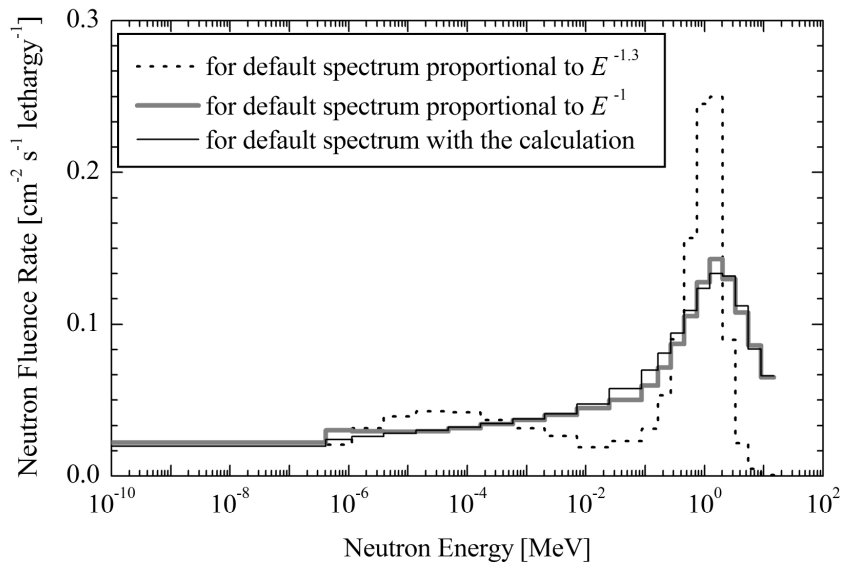

Fig. 4.2.1.3   Trial unfolded spectra using the default spectra proportional to $E^{-1.3}$, E^{-1} and that determined by calculation.

44

4-2-2. High energy neutrons

As to energetic neutrons greater than 15 MeV, our results obtained with the phoswich detector were compared with calculations using three different codes, LUIN2000 (O'Brien 1978), EXPACS (Sato et al. 2008) and RMC (Takada et al. 2007) in Fig. 4.2.2.1.
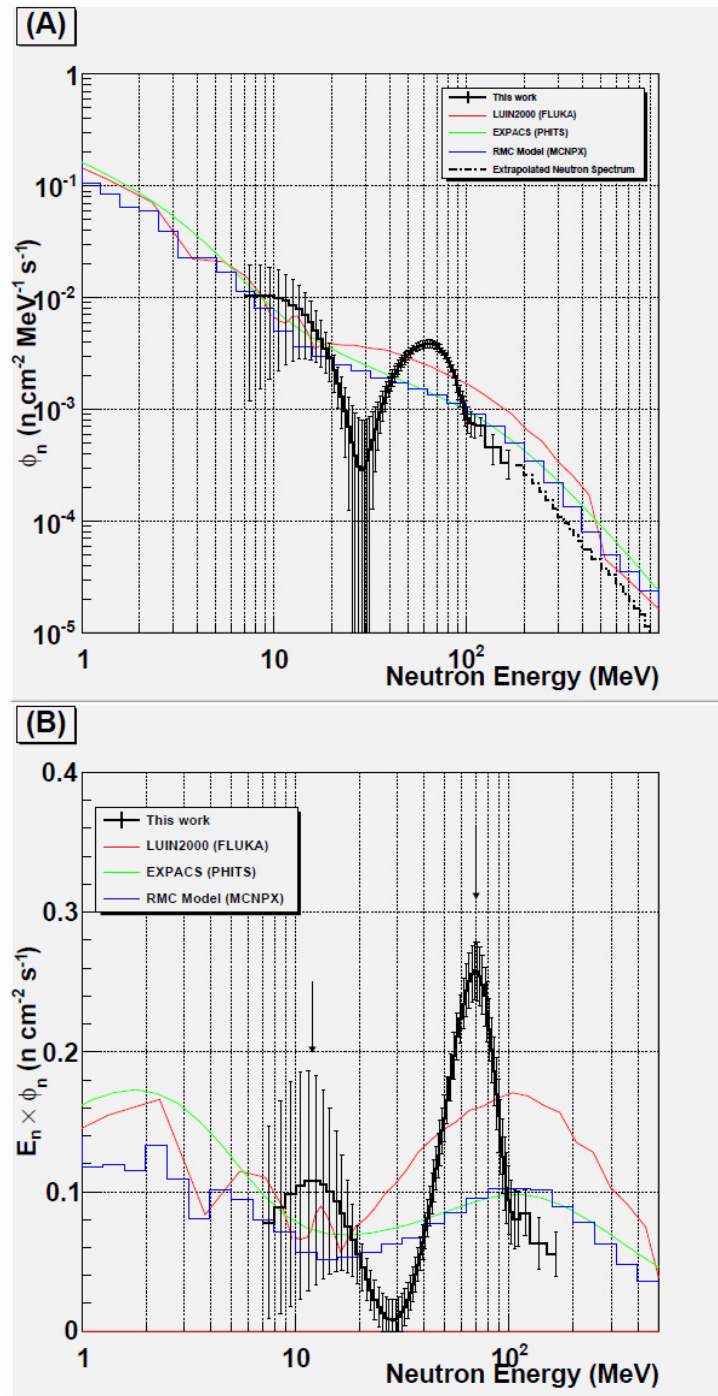

Fig. 4.2.2.1   Measured neutron energy spectrum compared with spectra calculated using

LUIN2000 (O'Brien 1978) based on a semi-empirical model, EXPACS (Sato et al. 2008) based on PHITS (Iwase et al. 2002) and RMC (Takada et al. 2007) based on MCNPX. The plots of (A) and (B) show the neutron flux and the spectrum multiplied by the neutron energy (i.e., the lethargy spectrum), respectively.

LUIN2000 calculates the neutron energy spectrum from the FLUKA-simulated neutron spectrum (Roesler et al. 1998) patched on the Hess neutron energy spectrum using the Chapman function (O'Brien 1978). EXPACS calculates the neutron energy spectrum using an analytical fitting formula based on the PHITS simulation. The RMC model uses a Microsoft Excel lookup table based on the MCNPX simulation. The plotted three high-energy neutron spectra at energies above 10 MeV were calculated using the FLUKA, PHITS, and MCNPX codes for the LUIN2000, EXPACS, and RMC codes, respectively. The calculations were performed at the same atmospheric depth, cut-off rigidity, and solar activity as our measurements. The EXPACS and RMC calculations give the same broad peak around 100 MeV and agree well with the Bonner ball measurements. However, they do not yield the sharp peak around 70 MeV. The LUIN2000 code gives results twice as large as the other calculated results.

The calculated neutron spectra were also integrated in several energy ranges, as shown in Table 4.1.4.1. The LUIN2000 calculated results show good agreement with our results in the peak region of 30 to 100 MeV but the former has 76% larger flux than ours over the entire energy region. The EXPACS calculation agrees well with our results from 7 to 180 MeV but shows a 20% larger value, including the high-energy spectrum beyond 180 MeV, and is 27% lower in the peak region. The RMC code agrees well within 9%, with our measured flux over the entire energy region. These comparisons confirm that our measured neutron fluxes are very reasonable within 30% difference.

Neutrons are transported in air in a cascade of attenuation and production from the cosmic-ray proton spectrum. It is very difficult to include various atmospheric phenomena exactly. The differences in spectral shape between our results and the calculations may be caused by one or more of the following three reasons. One is the uncertainty in the neutron cross sections used in nuclear data libraries and physical models, because neutron-nucleus reactions have not been evaluated sufficiently. Neutrons are produced in the atmosphere by particles with energies greater than 10 GeV, but no cross-section data for these high-energy neutrons are included in the LA150 (Chadwick et al. 1999) and JENDL/HE (Watanabe et al. 2005) data libraries. In this energy region, physical models are typically used to calculate the neutron and proton cross sections with atmospheric nuclei, but the physical models might yield uncertainty in neutron-nucleus reactions. The second is the geomagnetic conditions. The geomagnetic field has a strong angular dependence (Clem et al. 2003) which results in a large

difference in the cut-off sky map and typical vertical cut-off rigidity. The third is the source spectra of cosmic-ray protons and helium ions. The present work implies that those models and databases of primary cosmic-ray particle production shall be improved. Further investigation is continued.

5. Summary

5-1. Conclusion

The results obtained with commercial neutron dosemeters, so called rem counters (NCN1, WENDI-II and PRESCILA) gave remarkably different values of cosmic radiation dose at aviation altitude because of the sensitivity difference. Thus, we should be careful regarding the energy characteristics of the dosemeters employed, with particular attention being paid to the response functions for high-energy neutrons and also energetic charged particles such as protons and muons.

Neutron energy spectrum and dose at aviation altitude were obtained in the wide energy range from thermal to about 200 MeV by using two detectors, BBND (Bonner Ball Neutron Detector) and Phoswich detector. By using the Phoswich detector, we could obtain the first experimental neutron energy spectrum above 10 MeV and simultaneously photon energy spectrum up to 50 MeV with high energy resolution. A sharp neutron peak around 70 MeV obtained by the Phoswich detector is quite different from a broad neutron peak around 100 MeV by the previous Bonner ball experiments. Our results compared with calculations showed that the PHITS-based analytical radiation model PARMA gave an overestimated value to the BBND experiment in the neutron energy range below 15 MeV, while it gave an underestimated value to the Phoswich experiment around a 70 MeV peak region. These discrepancies are possibly due to uncertain environmental conditions inside and outside the aircraft.

5-2. Perspectives

It is desirable to reconfirm the reproducibility of the newly observed sharp peak around 70 MeV in future experiments. The peak position is considerably lower than those (about 100 MeV) reported in previous Bonner ball measurements, while some measurements with an organic liquid scintillator on the ground and with double-scatter neutron telescope at the top of atmosphere showed similar-position peaks.   Though the discrepancy of this finding compared to previous studies was discussed here in comparison with model simulations, further discussion is strongly required by performing onboard long-haul flight measurements at high geomagnetic latitude over north pole and south pole regions.

Such measurements will make the spectrometer very useful also for dosimetry of space radiation exposure of astronauts.   To achieve it, we need a more sophisticated detector regarding safety, energy efficiency and transportability, as well as the measurement precision of energetic cosmic-ray particles.   We now continue the efforts to develop such novel instruments, hoping to load it on the International Space Station.

Acknowledgements

References

Armstrong, T. W., K. C. Chandler, J. Barish, Calculations of neutron flux spectra induced in the Earth's atmosphere by galactic cosmic rays, J. Geophys. Res., 78[16], 2715–2726 (1973).

Baba, M., Nauchi, Y., Iwasaki, T., Kiyosumi, T., Yoshioka, M., Matsuyama, S., Hirakawa, N., Nakamura, T., Tanaka, Su., Meigo, S., Nakashima, H., Tanaka Sh. and Nakao, N. Characterization of a 40–90 MeV 7Li(p,n) neutron source at TIARA using a proton recoil telescope and a TOF method. Nucl. Instr. Meth A428(2/3), 454–465 (1999).

Baba, M.: Quasi-Monoenergetic Neutron Sources. Proc. of Sci., Int. WS on Fast Neutron Detect. (2006),http://pos.sissa.it/cgi-bin/reader/conf.cgi?confid=25#session-0 (Data accessed: October 2009)

G. Battistoni, S. Muraro, P.R. Sala, F. Cerutti, A. Ferrari, S. Roesler, A. Fasso and J. Ranft: The FLUKA code: Description and benchmarking, Proceedings of the Hadronic Shower Simulation Workshop 2006, Fermilab 6-8 September 2006, M. Albrow, R. Raja eds., AIP Conference Proceeding 896, 31-49 (2007).

Chadwick, M.B., P.G. Young, S. Chiba, S.C. Frankle, G.M. Hale, H.G. Hughes, A.J. Koning, R.C. Little, R.E. MacFarlane, R.E. Prael and L.S. Waters: Cross-Section Evaluations to 150 MeV for Accelerator-Driven Systems and Implementation in MCNPX, Nucl. Sci. Eng.131[3], 293–328 (1999)

Clem, J.M., G.De. Angelis, P. Goldhagen and J.W. Wilson: Preliminary Validation of Computational Procedures for a New Atmospheric Ionizing Radiation (AIR) Model, Adv. Space Res., 32[1], 27–33 (2003).

European Radiation Dosimetry Group (EURADOS). Cosmic radiation exposure of aircraft crew: compilation of measured and calculated data, A report of EURADOS Working Group 5. Luxembourg : European Commission; (2004).

Federal Aviation Administration. CARI-6, Radiobiology Research Team web site, http://www.faa.gov/education_research/research/med_humanfacs/aeromedical/radiobiology/cari6/; (2008).

Fukahori, T., Watanabe, Y., Yoshizawa, N., Maekawa, F., Meigo, S., Konno, C., Yamano, N., Konobeyev, Yu., Chiba, S. JENDL High Energy File. J. Nucl. Sci. Technol., Suppl.2:25-30; (2002).

Ferrari, A., M. Pelliccioni and T. Rancati: Calculation of the radiation environment caused by galactic cosmic rays for determining air crew exposure. Radiat. Prot. Dosim. 93, 101-114 (2001).

Ferrari, A., M. Pelliccioni and R. Villari: Evaluation of the influence of aircraft shielding on the aircrew exposure through an aircraft mathematical model. Radiat. Prot. Dosim. 108, 91-105 (2004).

Ferrari, A., P. R. Sala, A. Fasso and J. Ranft, FLUKA: a multi-particle transport code, CERN 2005-10, INFN/TC_05/11, SLAC-R-773 (2005).

Goldhagen, P., M. Reginatto, T. Kniss, J.W. Wilson, R.C. Singleterry, I.W. Jones and W.Van Steveninck: Measurement of the energy spectrum of cosmic-ray induced neutrons aboard an ER-2 high-altitude airplane. Nucl. Instr. Meth., A476, 42–51 (2002).

Goldhagen, P., J.M. Clem and J.W. Wilson: The energy spectrum of cosmic-ray induced neutrons measured on an airplane over a wide rage of altitude and latitude, Radiat. Prot.Dosim.110, 387–392 (2004).

Gordon, M.S., P. Goldhagen, K.P. Rodbell, T.H. Zabel, H.H.K. Tang, J.M. Clem and P. Bailey: Measurement of the Flux and Energy Spectrum of Cosmic-Ray Induced Neutrons on the Ground. IEEE NS. 51[6], 3427–3434 (2004).

GSF National Research Center for Environment and Health. EPCARD, http://www.helmholtz-muenchen.de/epcard2/index_en.phtml; (2008).

Hess, W. N., H. W. Patterson, R. Wallace, E. L. Chupp: Cosmic-ray neutron energy spectrum, Phys. Rev., 116[2], 445–457 (1959).

Heliocentric Potentials for Recent Dates, Civ. Aerosp. Med. Inst. in Fed. Aviat. Adm., http://www.faa.gov/data_research/research/med_humanfacs/aeromedical/radiobiology/heliocentric/ (Data accessed: October 2009)

Honma, T. : Recent Status of the NIRS Cyclotron Facility: Proc. of 18th Int. Conf. on Cyclotrons and Their Applications, Giardini Italy, 137–139 (2007).

Iwase, H., K. Niita and T. Nakamura: Development of General-Purpose Particle and Heavy Ion Transport Monte Carlo Code. J. Nucl. Sci. Technol., 39[11], 1142–1151 (2002).

Koshiishi, H., Matsumoto, H., Chisiki, A., Goka, T. and Omodaka, T.: Radiat. Meas., 42, 1510 (2007).

Lewis, B.J., McCall, M.J., Green, A.R. et al., Radiat. Protec. Dosim., 93, 293 (2001).

Lewis, B.J., M. Desormeaux, A.R. Green, L.G.I. Bennett, A. Butler, M. McCall and J.C. Saez Vergara: Assessment of Aircrew Radiation Exposure by Further Measurements and Model Development. Radiat. Prot. Dosim., 111[2], 151–171 (2004).

Matsumoto, H., Goka, T., Koga, K. et al., Radiat. Meas., 33, 321 (2001).

MCNPX User's Manual, Los Alamos National Laboratory report, LA-CP-05-0369 (2005). Information on MCNPX at URL http://mcnpx.lanl.gov/. (Data accessed: October 2009)

Nakamura, T., Uwamino, Y., Ohkubo, T., Hara, A.: Altitude Variation of Cosmic-ray Neutrons. Health Phys., 53, 509-517 (1987).

Nakamura, T., T. Nunomiya and M. Sasaki: Development of active environmental and personal neutron dosimeters. Radiat. Prot. Dosim., 110[1/4], 169–181 (2004).

Nakamura, T., T. Nunomiya, S. Abe, K. Terunuma and H. Suzuki: Sequential Measurements of Cosmic-Ray Neutron Spectrum and Dose Rate at Sea Level in Sendai, Japan, J. Nucl. Sci. Technol. 42[10], 843–853 (2005).

Nakamura, T., Ibe, E., Baba, M., Yahagi, Y., Kameyama, H.: Terrestrial Neutron-Induced Soft Errors in Advanced Memory Devices, World Scientific Publ. Co., April, (2008).

Nakane, Y.; Harada, Y.; Sakamoto, Y.; Oguri, T.; Yoshizawa, M.; Takahashi, F.; Ishikura, T.; Fujimoto, T.; Tanaka, S.; Sasamoto, N.: Evaluation of energy response of neutron rem monitor applied to high-energy accelerator facilities. JAERI-Tech 2003-011:1-37 (2004).

O'Brien, K.: A Code for the Calculation of Cosmic Ray Propagation in the Atmosphere, EML-338 (update of HASL-275) (1978).

Olsher, R.H.; Hsu, H.-H.; Beverding, A.; Kleck, J. H.; Casson, W. H.; Vasilik, D. G.; Devine, R. T. WENDI: An improved neutron rem meter. Health Phys. 79(2):170-181 (2000).

Olsher, R. H., Seagraves, D. T., Eisele, S. L., Bjork, C. W., Martinez, W. A., Romero, L. L., Mallett, M. W., Duran, M. A., Hurlbut, C. R.: PRESCILA: A new, light weight neutron rem meter. Health Phys. 86(6):603-612 (2004).

Olsher, R. H. and McLean, T. D. High-energy response of the PRESCILA and WENDI-II neutron rem meters. Radiat. Prot. Dosim. 130(4):510-513; (2008).

Oyama, Y., Sekiyama, K. and Maekawa, H.: Spectrum weight function method for in-situ fast neutron and gamma-ray responses measurements in fusion integral experiments with an NE213 scintillation detector, Fusion Technol. 26[3], pt2, 1098 (1994).

Preszler, A.M., G.M. Simnett and R.S. White: Angular Distribution and Altitude Dependence of Atmospheric Neutrons From 10 to 100 MeV, J. Geophys. Res. 79[1], 17–22 (1974).

Roesler, S., W. Heinrich and H. Schraube: Neutron spectra in the atmosphere from interactions of primary cosmic rays. Adv. Space Res. 21, 1717–1726 (1998).

Reginatto, M., P. Goldhagen: MAXED, A Computer Code for the Deconvolution of Multisphere Neutron Spectrometer Data Using the Maximum Entropy Method, USDOS Report EML-595, Environmental Measurements Laboratory, U.S. Department of Energy (1998).

Reginatto, M., P. Goldhagen: MAXED, a computer code for maximum entropy deconvolution of multisphere neutron spectrometer data. Health Phys., 77[5], 579–583 (1999).

Reginatto, M., P. Goldhagen, S. Neumann: Spectrum unfolding, sensitivity analysis and propagation of uncertainties with the maximum entropy deconvolution code MAXED, Nucl. Instrum. Methods A, 476, 242–246 (2002)

Satoh, D., Sato, T., Shigyo, N. and Ishibashi, K.: SCINFUL-QMD: Monte Carlo based computer code to calculate response function and detection efficiency of a liquid organic

scintillator for neutron energies up to 3 GeV, JAEA-Data/Code, 2006-023 (2006).

Sato, T., Satoh, D., Endo, A. and Yamaguchi, Y.: Development of Dose Monitoring System Applicable to Various Radiations with Wide Energy Ranges, J. Nucl. Sci. Technol. 42(9), 768-778 (2005).

Sato, T. and K.Niita: Analytical functions to predict cosmic-ray neutron spectra in the atmosphere. Radiat. Res. 166, 544–555 (2006).

Sato, T., Satoh, D., Endo, A. and Yamaguchi, Y.: DARWIN: Dose Monitoring System Applicable to Various Radiations with Wide Energy Ranges, Radiat. Prot. Dosim. 126, 501-505 (2007).

Sato, T., H. Yasuda, K. Niita, A. Endo and L. Sihver: Development of PARMA: PHITS-based Analytical Radiation Model in the Atmosphere, Radiat. Res., 170, 244–259 (2008), http://phits.jaea.go.jp/expacs/ (Accessed: October 2010)

Schrewe, U. J.: Global measurements of the radiation exposure of civil air crew from 1997 to 1999, Radiat. Prot. Dosim., 91[4], 347–364 (2000).

Shin, K., Y. Uwamino and T. Hyodo: Propagation of errors from response functions to unfolded spectrum.   Nucl. Technol., 53, 78–85 (1981).

Takada, M., Taniguchi, S., Nakamura, T., Fujitaka, K.: Development of a Phoswich Detector to Detect Neutrons and Charged Particles for Space Application., IEEE Trans. on Nucl. Sci., 45, 888 (1998).

Takada, M., S. Taniguchi, T. Nakamura and K. Fujitaka: Neutron Spectrometry in a Mixed Field of Neutron and Proton with a Phoswich Neutron Detector. Part II. Application of the Phoswich Neutron Detector to Neutron Spectrum Measurements. Nucl. Instr. Meth., A465, 512–524 (2001).

Takada, M., S. Taniguchi, T. Nakamura, N. Nakao, Y. Uwamino, T. Shibata and K. Fujitaka: Characteristics of a Phoswich Detector to Measure Neutron Spectrum in a Mixed Field of Neutrons and Charged Particles. Nucl. Instr. Meth., A476, 332–336 (2002).

Takada, M., I. Awaya, S. Iwai, M. Iwaoka, M. Masuda, T. Kimura, S. Takgagi, O. Sato, T. Nakamura and K. Fujitaka: Progress Report on the Phoswich Neutron Detector to Measure High-Energetic Neutron Spectra Onboard an Aircraft and a Spacecraft. J. Nucl. Sci. Technol., Suppl.4, 399–402 (2004).

Takada, M. and T. Nakamura: A Phoswich Detector for High-Energy Neutrons. Radiat. Prot. Dosim., 126, 178–184 (2007).

Takada, M., B.J.Lewis, M.Boudreau, H.Al Anid and L.G.I.Bennett: Modelling of Aircrew Radiation Exposure from Galactic Cosmic Rays and Solar Particle Events, Radiat. Prot. Dosim. 124[4], 289–318 (2007).

Takada, M., K. Yajima, H. Yasuda, T. Nakamura, M. Baba, T. Homma, A. Endo and Y.

Tanimura: Response Functions of Phoswich-Type Neutron Detector for High-Energy Cosmic-Ray Neutron Measurement. J. Nucl. Sci. Technol. **47**, 917-931 (2010).

Takada, M., K. Yajima, H. Yasuda, T. Sato and T. Nakamura: Measurement of Atmospheric Neutron and Photon Energy Spectra at Aviation Altitude using a Phoswich-type Neutron Detector. J. Nucl. Sci. Technol. **47**, 932-944 (2010).

Watanabe, Y., T. Fukahori, H. Nakashima, S. Chiba, K. Kosako, N. Shigyo, T. Murata, N. Yamano, T. Hino and K. Maki: Nuclear Data Evaluations for JENDL High-Energy File, Proc. Int. Conf. on Nucl. Data for Sci. and Technol., Santa Fe, New Mexico, USA, Sept. 26 - Oct. 1, 2004, 1, 326–331 (2005).

Yajima, K., Yasuda, H., Takada, M., Sato, T., Goka, T., Matsumoto, H. and Nakamura, T.: Measurements of Cosmic-Ray Neutron Energy Spectra From Thermal to 15 MeV with BBND in Aircraft. J. Nucl. Sci. Technol., 47[1], 31–39 (2010).

Ziegler, Z.F.: Terrestrial cosmic ray intensities. IBM. J. Res. Develop. 42, 117-139 (1998).

Research Outputs related to the Present Study

Original Papers

O-1. Kazuaki Yajima and Hiroshi Yasuda: Measurement of cosmic-ray origin neutrons using a scintillation detector at the summit of Mt.Fuji. Radiat. Meas. 46: 1724-1727, 2011.

O-2. Tatsuhiko Sato, Koji Niita, V. A. Shurshakov, B.E. Kalyaev, E.N. Yarmanova, I.V. Nikolaev, Hiroshi Iwase, Lembit Sihver, D. Mancusi, Akira Endo, N. Matsuda, Yousuke Iwamoto, Hiroshi Nakashima, Yukio Sakamoto, Hiroshi Yasuda, Masashi Takada and Takashi Nakamura. Applications of the PHITS code to space researches: estimation of dose reduction rate due to water shielding in front of Russian crew cabin. Cosmic Research. 49:319-324, 2011..

O-3. Hiroshi Yasuda, Kazuaki Yajima, Satoshi Yasuda: Dosimetry of cosmic radiation in the troposphere based on the measurements at the summit of Mt. Fuji. Proc. Radiochim. Acta, 1:67-70, 2011.

O-4. Hiroshi Yasuda, Tatsuhiko Sato, Hidenori Yonehara, Toshiso Kosako, Kazunobu Fujitaka, Yasuhito Sasaki: Management of cosmic radiation exposure for aircraft crew in Japan. Radiat. Prot. Dosim. 146:123-125, 2011.

O-5. Hiroshi Yasuda, Jaejin Lee, Kazuaki Yajima, Jung A Hwang, Kazuo Sakai: Measurement of cosmic-ray neutron dose onboard a polar route flight from New York to Seoul. Radiat. Prot. Dosim. doi: 10.1093/rpd/ncr152, 2011.

O-6. Hiroshi Yasuda, Kazuaki Yajima, Masashi Takada, Tatsuhiko Sato, Takashi Nakamura: Development of Cosmic Radiation and Energetic Particle Analysing System :CREPAS. Prog. Nucl. Sci. Technol., 1: 356-358, 2011.

O-7. Tatsuhiko Sato, Akira Endo, Hiroshi Yasuda et al. Fluence-to-dose conversion coefficients for aircrew dosimetry based on the new ICRP recommendations. Prog. Nucl. Sci. Technol. 1: 134-137, 2010.

O-8. Hiroshi Yasuda, Kazuaki Yajima: Characterization of radiation instruments at the summit of Mt. Fuji. Radiat. Meas. 45: 1600-1604, 2010.

O-9. Kazuaki Yajima, Hiroshi Yasuda: Measurement of cosmic-neutron energy spectrum at the summit of Mt. Fuji. Radiat. Meas. 45: 1597-1599, 2010.

O-10. Kazuaki Yajima, Hiroshi Yasuda, Masashi Takada, Tatsuhiko Sato, Tateo Goka, Haruhisa Matsumoto, Takashi Nakamura: Measurements of cosmic-ray neutron energy spectra from thermal to 15 MeV with Bonner Ball neutron detector in aircraft, J. Nucl. Sci. Technol. 47:31-39, 2010.

O-11. Vladimir Mares, Hiroshi Yasuda: Aviation route doses calculated with EP-CARD.Net and JISCARD EX. Radiat. Meas. 45: 1553-1556, 2010.

O-12. Masashi Takada, Kazuaki Yajima, Hiroshi Yasuda, Takashi Nakamura, Mamoru Baba, Toshiso Honma, Akira Endo, Yoshihiko Tanimura: Response functions of phoswich-type neutron detector for high-energy cosmic ray neutron measurement, J. Nucl. Sci. Technol. 47: 917-931, 2010.

O-13. Masashi Takada, Kazuaki Yajima, Hiroshi Yasuda, Tatsuhiko Sato, and Takashi Nakamura: Measurement of Cosmic Neutron and Photon Energy Spectra on Board an Aircraft Using a Phoswich-Type Neutron Detector. J. Nucl. Sci. Technol. 47: 932-944, 2010.

O-14. Masahi Takada, Kazuaki Yajima, Hiroshi Yasuda, Tatsuhiko Sato and Takashi Nakamura: Neutron, Photon and Proton Eenergy Spectra at High Altitude Measured using a Phoswich-Type Neutron Detector. Radiat. Meas. 45(10): 1297-1300, 2010.

O-15. Kazuaki Yajima, Hiroshi Yasuda, Masashi Takada, Tateo Goka, Haruhisa Matsumoto and Takashi Nakamura. Measurement of Low to Middle Energy Neutron Spectra at Aviation Altitude. J. Nucl. Sci. Technol. 47:31-39, 2010.

O-16. Tatsuhiko Sato、Daiki Satoh、Akira Endo、Nobuhiro Shigyo、Hiroshi Yasuda、Masashi Takada、Kazuaki Yajima、Takashi Nakamura: The Recent Improvement and Verification of DARWIN: Development of a New DAQ System and Results of Flight Experiment. Nucl. Technol. 168:113-117, 2009.

O-17. Hiroshi Yasuda, Kazuaki Yajima, Tatsuhiko Sato, Masashi Takada and Takashi Nakamura. Responses of Selected Neutron Monitors to Cosmic Radiation at Aviation Altitude. Health Phys. 96:655-660, 2009.

O-18. Tatsuhiko Sato, Hiroshi Yasuda, Koji Niita, Akira Endo and Lembit Sihver, Development of PARMA: PHITS-based analytical radiation model in the atmosphere. Radiat. Res. 170:244-259, 2008.

O-19. Tatsuhiko Sato, Daiki Satoh, Akira Endo and Yasuhiro Yamaguchi. DARWIN: Dose Monitoring System Applicable to Various Radiations with Wide Energy Ranges. Radiat. Prot. Dosim. 126: 501-505, 2007.

O-20. Masashi Takada and Takashi Nakamura. A Phoswich Detector for High-Energy Neutrons. Radiat. Prot. Dosim. 126: 178-181, 2007.

O-21. Hiroshi Yasuda. Space Radiation Dosimetry by Combination of Integrating Dosemeters. Radiat. Prot. Dosim. 120:410-413, 2006.

Reviews

R1. Tateo Goka, Kiyokazu Koga, Haruhisa Matsumoto, Tatsuto Komiyama and Hiroshi Yasuda: Radiation Environment in Space. Jpn. J. Health Phys. 46(1): 31-41, 2011. (in Japanese)

R2. Hiroshi Yasuda: Effective dose measured with a life-size human phantom in a low Earth orbit mission. J. Radiat. Res. 50: 89-96, 2009.

R3. Hiroshi Yasuda: Exposures to neutrons at high altitude. Ionizing Radiation 31(4): 299-312, 2005. (in Japanese)

Books

B1. Takashi Nakamura, Eishi Yahagi, Hideaki Kameyama, Yasuo Yahagi, Mamoru Baba: Terrestrial Neutron-Induced Soft Errors in Advanced Memory Devices. World Scientific Publication Co. Inc., ISBN-10: 9812778810, 2008.

Awards

A1. Masashi Takada, Hiroshi Yasuda, Kazuaki Yajima: Atomic Energy Society of Japan 44th Excellent Research Paper Award (日本原子力学会・第 44 回論文賞), 2012.

A2. Takashi Nakamura: Atomic Energy Society of Japan 43th Scientific Achievement Award (日本原子力学会・第 43 回学術業績賞), 2011.

A3. Hiroshi Yasuda: The 1st Award of the Asian Association for Radiation Research (アジア放射線研究連合 第 1 回アジア賞), 2009.

A4. Takashi Nakamura: Japan Health Physic Society 2007 Achievement Award (日本保健物理学会・平成 19 年度功労賞), 2007.

和文要約（Summary in Japanese）

航空機内における宇宙線中性子の線量及びスペクトルの評価

　宇宙船や航空機に搭乗中に経験する宇宙線環境の正確な把握は、搭乗する乗員の放射線防護にとって重要な課題である。彼らは、幅広いエネルギーを持つ様々な種類の宇宙線粒子に被ばくする。それらの粒子は乗員の体内において複雑な反応を起こし、深部臓器で起こる反応が健康に重大な影響を及ぼす可能性がある。この影響について論じ評価するには、特に線量寄与が大きいと考えられる高エネルギー中性子など透過力の強い粒子成分について、その正確なエネルギースペクトルを空間分布と共に知ることが必要である。しかしながら、陽子やミュー粒子等が少なからず混在する高高度の環境において、10~20 MeV を超える中性子を荷電粒子と明確に区別して正確なエネルギースペクトルを測ることは困難である。

　このような背景の下、我々は、平成 18（2006）年から 20（2008）年の太陽活動極小期において、ビジネスジェット機を利用して高高度において宇宙線中性子の測定実験を8 回実施し、新たな測定技術の検証に取り組んだ。航空機の利用にあたっては、宇宙航空研究開発機構（JAXA）が管轄する事業として財団法人日本宇宙フォーラムが運営した公募研究「第 8 回宇宙環境利用に関する地上研究」（平成 17～19 年度、研究代表者: 中村尚司）の支援を受け、ダイアモンド エア サービス株式会社の協力を得た。

　宇宙線中性子の測定には、独自に新規開発した中性子スペクトロメータを含め、複数の放射線測定器を使用した。その新しいスペクトロメータは、性質の異なるシンチレータを組み合わせたフォスウィッチ型のシンチレーション検出器で、10 MeV から約 200 MeV までの中性子を弁別して検出し、そのエネルギースペクトルを評価できる性能を持つものである。本研究の主要な目的の 1 つは、当該測定器の有効性を高高度の宇宙線環境において確認することにあった。

　中性子レムカウンタを用いた実測の結果から、PHITS をベースにした解析モデル（PARMA）を用いて宇宙線中性子の線量を精度よく推定できることが検証された。又、新規開発したスペクトロメータを用いて高エネルギー（10～200 MeV）中性子のスペクトルを評価できることが確認された。得られた 10 MeV 以上のスペクトルと別途ボナーボール測定装置で評価された 15 MeV 以下のスペクトルとの連続性は良好であった。本実験は、民間ジェット機の飛行高度において、熱エネルギー領域から高エネルギー領域までの中性子のエネルギースペクトルを高分解能で実測・評価することに成功した世界初の実験である。

一方、本実験で用いたスペクトロメータにより得られた結果では、高エネルギー中性子のピークが 70 MeV 近辺に見られた。この結果は、地上における有機液体シンチレータ及び地球大気最上層における二重散乱テレスコープによる測定結果とは一致するものの、過去にボナーボール検出器で測定評価された高エネルギー中性子のピーク（約 100 MeV）よりも顕著に低いものである。

　このピーク位置に関する妥当性や本研究で得られた新しい結果の信頼性について論じるには、宇宙線強度の強い高緯度での長距離飛行や、可能であれば国際宇宙ステーションの与圧部内において同様の測定を行い、実験結果の変動や再現性等を確認することが必要である。その際には、安全かつ省電力で持ち運びが容易な、より洗練された測定装置を準備する必要があり、現在その作業に取り組んでいるところである。

平成 23 年 12 月

(独)放射線医学総合研究所
　　保田浩志、高田真志、矢島千秋
(独)日本原子力研究開発機構
　　佐藤達彦
(財)日本宇宙フォーラム
　　藤島　徹
東北大学
　　中村尚司

National Institute of Radiological Sciences